CHARACTERISTICS OF VERTICAL STRONG GROUND MOTIONS FOR APPLICATIONS TO ENGINEERING DESIGN*

Walter Silva, Pacific Engineering and Analysis
311 Pomona Avenue, El Cerrito, CA 94530

Introduction

In the near-source region (D ≤ 10 to 15 km) of large earthquakes, the characteristics of strong ground motions change in stable and predictable ways: durations become significantly shorter (Chang et al., 1996; Abrahamson and Silva, 1997), velocity and displacement time histories can increase significantly in amplitude and become more pulse like (depending upon rupture directivity effects), long period fault normal motions show a stable increase over fault parallel motions (Somerville et al., 1997), and short period vertical motions can exceed horizontal motions (Niazi and Bozorgnia, 1991; Bozorgina et al., 1995) at both rock and soil sites (EPRI, 1993).

For vertical motions, these recent observations suggest that the commonly adopted vertical-to-horizontal response spectral ratio of 2/3 (Newmark and Hall, 1978) may be significantly exceeded at short periods in the near-source distance range. With the increase in near-source strong motion recordings at both rock and soil sites to aid in constraining empirical attenuation relationships as well as providing direct estimation of statistical spectral shapes for vertical and horizontal components, it is possible to examine the dependencies of the vertical-to-horizontal response spectral ratio (V/H) on magnitude, distance, and site conditions.

As an additional and important aspect, similarities and differences in the characteristics of the time histories between vertical and horizontal motions can be examined. For design motions, the relative phasing between horizontal and vertical motions can be an important issue, leading to different structural analyses and design decisions depending on whether or not significant energy is expected to occur both vertically and horizontally at or nearly the same time.

Effects of Site Conditions on the Characteristics of Vertical and Horizontal Strong Ground Motions

To broadly classify strong motion recordings sites into rock or soil, the Geomatrix categorization criterion listed in Table 1 is used. While the distinction between rock and soil is becoming less clear for Western United States (WUS) sites as more rock sites are drilled and velocities determined (EPRI, 1993; BNL, 1997), this largely qualitative classification scheme does capture significant and stable differences in strong ground motions (Sadigh et al., 1997; Abrahamson and Silva, 1997; BNL, 1997).

---

* Silva, W.J. (1997). "Characteristics of vertical strong ground motions for applications to engineering design." *Proc. Of theFHWA/NCEER Workshop on the Nat'l Representation of Seismic Ground Motion for New and Existing Highway Facilities,* I.M. Friedland, M.S Power and R. L. Mayes eds., Technical Report NCEER-97-0010.

Generic Rock and Soil Site Velocity Profiles

To have an appreciation for the compression- and shear-wave velocity profiles implied by the rock and soil categories (Table 1), Figures 1 and 2 show median (lognormal distribution) and $\pm$ 1 σ velocity profiles computed for the two categories. The velocity profiles were computed from measured (downhole or crosshole) velocities at strong motion sites classified as Geomatrix A or B (Figure 1) or C or D (Figure 2). For the generic rock site, a strong velocity gradient is seen in the top 150 ft with low near-surface shear- and compression-wave velocities: approximately 800 ft/sec and 1,600 ft/sec respectively. The shear-wave velocity value of about 800 ft/sec departs significantly from the classically assumed value of about 2,500 ft/sec which is apparently not reached, on average, until a depth of about 70 to 100 ft. With such low near- surface velocities, these rock sites may be expected to show some nonlinear effects under very high loading conditions (BNL, 1997).

The absolute variability of both the shear- and compression-wave velocities is high (COV 0.5 to 0.6) and there is little to suggest the presence of the water table at a compression-wave velocity of about 5,000 ft/sec. Contrasting the rock site profiles in Figure 1 with those of the soil in Figure 2, significant differences are immediately apparent. Interestingly, over the top 50 ft or so, the compression-wave velocities are very similar for both the rock and soil sites. For the soil site, with the much lower shear-wave velocities, a significantly higher Poission's ratio is implied reflecting a larger Vp/Vs ratio for soil than for rock. Additionally for the soil site, the effect of the water table on the compression-wave velocity is apparent in the nearly constant velocity of the fluid phase at about 5,000 ft/sec at depths from around 100 ft to 250 ft. Beyond about 200 ft, the compression-wave velocity of the skeleton material exceeds that of the fluid phase which is reflected in the velocity increase with depth.

The velocity variability at the soil site, although much less in absolute variation, is similar to that of the rock site in a relative sense ($\sigma_{ln} \approx 0.4$ to 0.5). This suggests that strong ground motions may be more variable at rock than at soil sites.

To contrast the dynamic material properties between rock and soil sites further, Figures 3 and 4 show Poisson's ratios computed from the compression- and shear-wave velocity profiles. The higher variability in dynamic material properties for the rock verses the soil sites is reflected in the larger variation in Poisson's ratio for the rock site (Figure 3 verses Figure 4). The rock site has the lower overall Poisson's ratio which increases with depth to about 70 ft, remains nearly constant to a depth of about 200 ft, and then decreases to a value near 0.25 at a depth of 500 ft. Interestingly, Poisson's ratio for the soil site (Figure 4) shows a similar trend but shifted nearly a constant amount to a depth of about 350 ft. Beyond about 350 ft, Poisson's ratio for the soil site decreases less rapidly than for the rock site, remaining at a value of around 0.4 to a depth of 500 ft.

The dashed lines on Figures 3 and 4 represent smooth Poisson's ratio models and are shown in Figure 5 for the generic rock and soil sites. The similar patterns and nearly constant shift to a depth of about 350 ft are quite apparent in the smooth models.

The differences in Poisson's ratio as well as the overall velocities between the rock and soil sites may have important implications for the differences in vertical and horizontal motions. At rock sites, even though the shallow shear-wave velocities are low, the steep velocity gradient results in shear-

wave velocities exceeding 2,000 to 3,000 ft/sec at depths of 50 to 70 ft. As a result, for the same level of control (input motions), nonlinear effects are expected to be much less pronounced than at a corresponding soil site and generally confined to the top 50 to 100 ft. The higher rock velocities and shallower potentially nonlinear zone will also tend to confine nonlinear effects to higher frequencies (BNL, 1997). If vertical motions are more linear than horizontal, perhaps due to lower strains for inclined SV-waves and contributions of P-waves, the magnitude dependence of the V/H ratio would be expected to be less at rock sites than at soil sites. As magnitude increases, the higher loading levels induce more nonlinearity in the horizontal motions at soil sites than the rock sites. The vertical motions, remaining relatively linear, simply scale up and broaden in spectral content as magnitude increases. As a result, the magnitude scaling of the V/H ratios should be inversely proportional to the profile stiffness: significantly larger for soil than for rock conditions.

In addition to the effects of overall stiffness, the large jump in Poisson's ratio at the soil/rock interface (or steep gradient) at soil sites (Figure 5) will have an important impact on incoming wavefields. For a generic California deep crustal model, the average shear- and compression-wave velocities at the surface are about 3,500 to 4,500 ft/sec and 6,500 to 8,000 ft/sec (BNL, 1997). For a deep generic soil site, Figure 2 shows shear- and compression-wave velocities at a depth of 500 ft of about 2,000 ft/sec and 6,500 ft/sec respectively. Transition to rock at this depth then would likely involve a very steep shear-wave velocity gradient with a factor of 2 or more jump in velocity. For the compression-wave, the transition is much less pronounced, a factor of only 1.0 to 1.2 on average. This consequence of the drop in Poisson's ratio in transiting from soil to rock, being manifested in a large jump in shear-wave velocity, will tend to refract (bend) incident shear-waves much more severely than incident compression-waves. In passing through the rock/soil transition zone, the incident shear-waves will become much more vertical than the incident compression-waves. For incident SV-waves, this will have the effect of converting vertical motions to horizontal motions while the compression-waves largely remain inclined until depths of 100 to 200 ft where they are amplified and refracted (bent to a more vertical incidence) by the shallow compression-wave gradient (Figure 2).

Since earthquake sources emit much larger shear-wave amplitudes than compression-wave amplitudes, by the ratio of the source region velocities cubed ($(Vp/Vs)^3 \approx 5$), incident inclined SV-waves may be expected to dominate vertical motions at close distances. At large distances, the SV-wave is beyond its critical angle and does not propagate to the surface very effectively (Kawase and Aki, 1990). At a source depth of 8 km and a average or generic California crustal model (Figure 31) the SV-wave critical angle for geometrical ray theory occurs at an epicentral distance of about 5 km for a point-source. Crustal heterogeneity and source finiteness (vertical extent) would tend to extend this distance somewhat. Also, geometrical ray theory is appropriate for high frequencies and low frequency energy would tend to be refracted less by the shallow velocity gradients, also resulting in extending the distance to the SV-wave critical angle. However, even considering these effects, the SV-wave is not likely to dominate the vertical component at distances exceeding 10 to 20 km.

At soil sites, due to the large change in shear-wave velocity at the base of the profile and the accompanying wave refraction, compression-waves may be expected to dominate the vertical motions at near as well as far distances. Additionally, because of the large compression-wave velocity gradient from the surface to depths of about 100 to 200 ft, short period compression-waves will be amplified which will result in large short period vertical motions.

Short-Period Time Domain Characteristics of Vertical Motions

To illustrate the effects of site conditions on acceleration time histories for vertical and horizontal components, a series of plots from the CDMG initial earthquake data reports are presented. These plots show all three components for each site in a convenient format for illustrative purposes.

To consider first close-in rock sites, Figure 6 shows three component acceleration time histories at the Pacoima Dam (Downstream) and Corralitos sites for the 1994 **M** 6.7 Northridge and 1989 **M** 6.9 Loma Prieta earthquakes. Both sites are within about an 8 km fault distance and both sets of records show very similar motions on the horizontal and vertical components. Structures founded on rock conditions at close distances may then be expected to experience simultaneous horizontal and vertical demands at similar levels and over a fairly broad period range.

For close-in soil sites, Figure 7 shows distinctly different features in the Sylmar County Hospital and Arleta records for the Northridge earthquake. As for the rock sites, the soil sites are close-in recordings at fault distances of 6.1 km for Sylmar and 9.2 km for Arleta. Unlike the rock site recordings however, the soil site records show strong short-period motion arriving significantly before the large horizontal motions. Structures founded on deep soil would then be expected to experience vertical and horizontal demands significantly different than on rock conditions. The vertical demands at close-in soil sites would generally be characterized as out of phase with the dominant horizontal motions and of much higher frequencies. The largest short period motions on the vertical component may arrive before those of the horizontal and will be larger than the short period horizontal motions. During the passage of the dominant horizontal component motions, the vertical demands on a structure could be characterized as random high- frequency chatter which may exceed 1g at short periods. This is markedly different than the vertical motions at close-in rock sites, which tend to show strong low frequency coherence with the horizontal motions.

For the more distant sites, Figure 8 shows some interesting features across the Gilroy array for motions due to the 1989 Loma Prieta earthquake. Rock sites Gilroy 6 and 7, at fault distances of 19.9 and 24.2 km respectively, show features similar to those at the close-in soil site: earlier arriving and high-frequency vertical motions out-of-phase with the dominant horizontal motions. At rock site Gilroy 1 however, at a fault distance of 11.2 km, the vertical motions display early arriving high frequency energy as well as low-frequency energy coherent with the dominant horizontal motions. A possible explanation for this behavior is that this site, at a fault distance of about 11 km, is in the transition region from close-in to more distant rock site characteristics.

An interesting and apparent contradiction to the expected close-in rock site characteristics are the recordings at Pacoima Kagel Canyon for the Northridge earthquake (Figure 9). This rock site is at a fault distance of 8.2 km, about the same distance as the Pacoima Downstream site (Figure 6), but displays soil site characteristics on the vertical component: early arriving high frequency energy and out-of-phase motions with the horizontal components. As part of a recent, Caltrans/NSF/EPRI sponsored project to Resolve Site Response Issues Associated with the Northridge Earthquake (ROSRINE), this recording site, as well as many others, has recently been drilled and logged. Based on the shear-wave velocity logging, the site is misclassified. With shear-wave velocities of just under 2,000 ft/sec from about 100 ft to the bottom of the hole at about 300 ft, the site is closer to a

stiff soil than rock (Figures 1 and 2). This is not entirely unexpected being comprised of the Saugus formation, a typically soft Los Angeles area sandstone.

For the distant (D ≥ 10 to 15 km) soil sites, Figure 10 shows the remaining sites across the Gilroy array which recorded the Loma Prieta earthquake. Site Gilroy 2 is at fault distance of 10.7 km and sites 3 and 4 are at fault distances of 14.4 and 16.1 km respectively. As with the close-in soil sites (Figure 7) and the distant rock sites (Figure 8), the vertical motions show high frequency early arriving energy and little coherence with the dominant horizontal motions.

These acceleration time history plots are intended to illustrate general trends in short period vertical and horizontal motions. The intent is to show dominately SV motion, for close distances (≤ 10 to 15 km) on the vertical component with similar phasing as the horizontal components for rock sites while at soil sites, compression-waves dominate the vertical motions showing earlier arriving and larger higher frequency energy content. At more distant sites, compressional-wave energy tends to be dominant on the vertical component at both rock and soil sites.

Response Spectral Characteristics of Vertical Motions

To examine distance and site condition dependencies of vertical motions in more detail, as well as broader period range, Figures 11 to 18 show 5% damped pseudo absolute response spectra as well as acceleration, velocity, and displacement time histories for a selected set of sites. Cases examined are close-in and more distant rock and soil sites. Acceleration, velocity, and displacement time histories are plotted to show that at close-in soil sites and at more distant rock and soil sites, long period coherence exists between vertical and horizontal components. This results in the dominant long period motions being "in-phase" in the sense that the largest long period motions occur around nearly the same time on both the vertical and horizontal components.

For the close-in rock site, Figure 11 shows response spectra computed for the vertical and two horizontal component records at the Southern California Edison Lucerne site from the 1992 **M** 7.2 Landers earthquake. The fault distance is about 2 km and the vertical component slightly exceeds the horizontal components at periods shorter than about 0.1 sec. At long periods, beyond about 1 sec, the vertical is comparable to the smaller of the horizontal components, the fault-parallel motion. The period range of nearly constant spectral acceleration in the horizontal components, about 2 to 5 sec, is likely due to the effects of directivity.

The corresponding time histories are shown in Figure 12 and reveal strong coherence among components. The maximum velocity and displacement of the vertical component exceed those of the fault-parallel component. The maximum vertical displacement is about 15 cm or about 6 inches occurring over a 2 sec period of time during which the fault-normal direction moved nearly 2 feet (≈ 60 cm).

For the close-in soil site, Figures 13 and 14 show the response spectra and time histories at the Arleta site for the 1994 Northridge earthquake. The fault distance is 9.2 km and the vertical component greatly exceeds the horizontal components at periods shorter than about 0.2 sec. Beyond about 2 sec, as with the rock site Lucerne, the vertical component becomes comparable to the horizontal. The time histories are shown in Figure 14 and indicate long period coherence and out-of-phase short

period energy (Figure 7).

For the more distant sites, Figures 15 and 16 show response spectra and time histories for the Gilroy array no. 6 rock site and Figures 17 and 18 show corresponding plots for the Gilroy array no. 4 soil site. The earthquake is the 1989 Loma Prieta and the distances are 16.1 and 19.9 km for sites 4 and 6 respectively. For both sites, the short period vertical motions relative to the corresponding horizontal motions are significantly reduced compared to the close-in sites. Interestingly, as with the close-in sites, the long period vertical motions approach the horizontal motions for periods beyond about 2 to 4 sec. This feature is not predicted by either empirical or numerical modeling and suggests that vertical motions are associated with high variability.

The corresponding time histories, Figures 16 and 18, show the usual pattern; early arriving short period energy on the verticals, out-of-phase with the horizontal motions with longer period motions becoming more in-phase between the components.

Magnitude, Site, and Distance Dependencies of Horizontal and Vertical Component Response Spectral Shapes

To examine empirically the role of possible site nonlinearity in the V/H ratios, statistical spectral shapes (Sa/PGA) were computed for magnitude bins centered on **M** 5.5 and **M** 6.5 for both rock and soil sites. The magnitude bins are one-half unit wide (**M** 5.5 = **M** 5 - 6, **M** 6.5 = **M** 6 - 7+) to include enough records to produce smooth and stable shapes.

The distance range was truncated at 50 km to avoid the effects of distance dependencies on the shapes. Records were selected from the PE&A strong motion database which includes available strong motion data for **M** $\geq$ 4.5. For this application only earthquakes occurring in tectonically active regions were selected (the 1995 **M** 6.9 Kobe earthquake is included).

To examine the effects of the level of loading on the vertical and horizontal component spectral shapes, two distance bins were selected: 0 to 10 km and 10 to 50 km. For **M** 5.5 rock sites, Figure 19 shows the horizontal and vertical statistical shapes. To assess nonlinear effects, Figure 19 shows shapes computed for the two distance bins: 0 to 10 km and 10 to 50 km. The vertical spectral shapes (dashed lines) show more short period energy than the horizontal shapes (solid and dotted lines) and about the same level of maximum spectral amplification. The vertical shapes have a maximum spectral amplification near 0.1 sec whereas the shapes for the horizontal component peak near 0.2 sec. This difference is likely due to differences in damping with the vertical component showing significantly less damping than the horizontal. The lack of any significant distance dependency in this shift in peak spectral amplification between the vertical and horizontal components suggests that the differences in damping is occurring in the shallow portion of the path and that the sites are behaving in a linear manner as well. The shallow crustal damping is thought to occur in the top 1 to 2 km of the crust (Anderson and Hough 1984; Silva and Darragh, 1995) and is generally modeled as a frequency independent exponential damping term with a damping parameter termed kappa:

$$\kappa = \frac{H}{\overline{V_S}\ \overline{Q_S}}, \quad \overline{Q_S} = \frac{1}{2\,\overline{\eta_S}} \tag{1}$$

where H is the depth of the damping zone (1 to 2 km), $\overline{V_S}$ and $\overline{Q_S}$ are the average shear-wave velocity and quality factor over the depth H and $\overline{\eta_S}$ is the corresponding damping ratio (decimal).

Response spectral shapes depend strongly on kappa, shifting to shorter periods as kappa decreases (Silva and Darragh, 1995). To illustrate this effect, Figure 20 shows response spectral shapes computed using a simple point-source model with kappa values ranging from 0.006 sec to 0.160 sec. The shift in shape with kappa is easily seen and a peak near 0.2 sec is consistent with a kappa value of about 0.04 sec while a factor of two shift in the peak to about 0.1 sec corresponds to a similar shift in kappa value to about 0.02 sec. Interestingly, the factor of 2 shift in kappa for the verticals ($\kappa_V \approx \kappa_H/2$; EPRI, 1993) was also found by Anderson (1991) in a detailed analysis of vertical and horizontal motions recorded at rock sites. The kappa or shallow crustal damping effect is the likely mechanism controlling the large shift in spectral shapes between soft rock WUS spectral shapes and hard rock CEUS spectral shapes (Silva and Darragh, 1995) and will impact hard rock vertical spectral shapes as well as horizontal component shapes.

To continue the shape comparison for rock sites, Figure 21 shows horizontal and vertical shapes computed for **M** 6.5 (**M** 6.0 - 7+) at the two distance ranges: 0 to 10 km and 10 to 50 km. As with the **M** 5.5 shapes, there is a distinct shift in the peak amplification frequency between vertical and horizontal spectra of nearly 2. Also there does not appear to be a strong distance or loading level effect on either the vertical or horizontal shapes suggesting largely linear response at these ground motion levels.

To consider soil sites, Figures 22 and 23 show the vertical and horizontal response spectral shapes for **M** 5.5 (**M** 5.0 - 6.0) and **M** 6.5 (**M** 6.0 - 7+) earthquakes. As with the **M** 5.0 rock shapes, there is about a factor of two difference in the periods of maximum spectral amplification between the vertical (near 0.1 sec) and horizontal shapes (near 0.2 sec). Also there is no appreciable and stable shift in either the vertical or horizontal shapes with loading level (0 - 10 km or 10 - 50 km) reflecting largely linear response. Similar periods of peak amplification between rock and soil of about 0.2 sec for the horizontal and 0.1 sec for the vertical suggests similar low strain damping values at both rock and soil sites.

For the **M** 6.5 (**M** 6.0 - 7+) shapes, shown in Figure 23, the horizontal soil shapes show a well defined and broad-band shift between 10 to 50 km and 0 to 10 km. The horizontal shape for 10 to 50 km peaks near 0.2 sec while that for 0 to 10 km peaks near 0.3 sec, crosses the 10 to 50 km shape, and maintains the shift from 0.1 sec to nearly 10 sec. These characteristics are very similar to those shown in Figure 20 which illustrated the effects of kappa on response spectral shapes. These results suggest nonlinear response resulting in an overall increase in kappa from about 0.04 sec (linear soil response) to about 0.06 to 0.08 sec at the higher loading levels.

For the vertical component in Figure 23, a slight shift appears to be present between the shapes computed for the 0 to 10 km and 10 to 50 km bins but the shift is in the wrong direction and is not stable with period, crossing at about 0.1 and again near 2.0 sec. This is likely due to a sampling

problem with too few sites contributing to the close-in (0 to 10 km) shapes.

The analyses of response spectral shapes revealed several features of interest: 1) a consistent shift in shapes between vertical and horizontal components at both rock and soil sites indicating lower shallow crustal damping for vertical components by about a factor of about 2, 2) similar low-strain damping values for rock and soil sites, and 3) horizontal component soil shapes show nonlinear response characterized by a stable and broad-band shift in shape to longer periods at higher loading levels. These features will be important factors in understanding the effects of magnitude, distance, and site condition on vertical-to-horizontal response spectral ratios.

Empirical and Numerical Model Estimates of the Vertical-to-Horizontal Response Spectral Ratios

To provide estimates of vertical-to-horizontal ratios as functions of magnitude, distance, and site conditions, a combination of empirical attenuation relations and numerical modeling is used. While the empirical relations are reasonably well constrained for WUS (or tectonically active regions), little data exist for **M** greater than 5.0 for CEUS conditions at distances of interest ($D \leq 20$ km).

The only large magnitude earthquake considered representative of the CEUS and which generated close-in strong motion records is the **M** 6.8 1985 Nahanni earthquake. It was recorded at only three sites, all hard rock, and all within 20 km of the source. This earthquake, along with smaller magnitude CEUS hard rock recordings, clearly show significantly different spectral content between WUS and CEUS horizontal rock motions. This feature is illustrated in Figure 24 which contrasts WUS and CEUS horizontal component rock site response spectral shapes for **M** around 6.5 and 4.0. The difference in short period spectral content between WUS and CEUS is significant and consistent between different magnitude earthquakes and is attributed to differences in shallow crustal damping or kappa values (Silva and Darragh, 1995). For CEUS rock site vertical components, an open question exists as to whether they show a shift to even shorter periods than the horizontal components (see Figure 21 for WUS rock). The effective bandwidth of current recordings is not capable of resolving this issue, however if similar physical mechanisms are controlling the motions at WUS and CEUS rock sites, some degree of shift would be expected and should be reflected in estimates of CEUS V/H ground motion ratios.

These differences in rock site spectral content may also have implications to soil motions since WUS and CEUS control motions, as well as rock outcrop motions, would be expected to have differences in spectral content. The differences in WUS and CEUS control motion spectral content may not result in significantly different deep soil horizontal motions due to the effects of material damping and nonlinearity. However, vertical component soil motions, if response remains largely linear in compression (constrained modulus), may have very high short period levels at close distances to large magnitude earthquakes (EPRI, 1993).

Applications to WUS Rock and Deep Soil Sites

For rock sites, the ratios reflect the average of Sadigh et al. (1997) and Abrahamson and Silva (1997) empirical relations, while for soil, because Sadigh et al. (1997) do not present a relationship for the vertical component, only Abrahamson and Silva (1997) relation is used. Figure 25 shows the

empirical vertical and horizontal spectra (5% damping) for **M** 6.5 at a distance of 5 km for both rock and soil site conditions. The shifting of the peak response of the vertical spectra to shorter periods than the horizontal is present showing a crossing in spectral levels at short periods. At this close distance (D = 5 km), response spectral ratios (V/H) would then exceed 1 at short periods and drop significantly at longer periods .

To look at the distance dependency of the V/H ratio for WUS, Figure 26 shows empirical ratios computed for both rock and soil sites. As expected, from the earlier examination of response spectra at individual sites (Figures 11, 13, 15, and 17), the maximum rock site V/H ratios are lower than the corresponding ratios for soil sites. For the rock sites, the distance dependency is considerably less than that for soil, a maximum of about 1.5 in going from 1 to 40 km. The larger distance dependence in the V/H ratios for soil sites may be due to nonlinear response of the soils: as distance increases relatively less damping is occurring in the soil column.

To look at the magnitude dependency of the empirical V/H ratios, Figure 27 shows ratios for rock and soil sites computed for distances of 1 and 20 km. The magnitude dependence of the V/H ratios is stronger for soil sites than for rock sites, again possibly reflecting effects of nonlinearity. Additionally, the magnitude dependence decreases with increasing distance for both rock and soil sites. For rock sites, this may be an artifact of the magnitude saturation built into the empirical relations, being different for rock and soil sites.

These empirical V/H ratios are reasonably well constrained and can provide the basis for developing smooth design ratios for WUS rock and deep moderately stiff soils. For applications to design motions, strong consideration should be given to adequate conservatism which should reflect the higher uncertainty in vertical motions compared to horizontal motions, particularly for close distances to large magnitude (**M** $\geq$ 7) earthquakes.

Applications to CEUS Rock and Deep Soil Sites

Based on the comparisons of the spectral content between WUS and CEUS rock site spectral shapes shown in Figure 24, differences in rock, and possibly soil V/H ratios may be expected to occur between the two tectonic regions (EPRI, 1993).

As previously discussed, due to the paucity of recordings (**M** $\geq$ 5, D $\leq$ 50 km) reflecting CEUS conditions, some form of modeling is necessary to assess the appropriateness of WUS V/H ratios for engineering design applications.

Computational Model

To model vertical motions, inclined P-SV waves from the stochastic point-source ground motion model (EPRI, 1993) are assumed and the P-SV propagators of Silva (1976) are used to model the crust and soil response to inclined P-SV wavefields. The angle of incidence at the top of the source layer is computed by two-point ray tracing through the crust and soil column (if present) assuming incident compression-waves.

To model soil response, a soil column is placed on top of the crustal structure and the incident

inclined P-SV wavefield is propagated to the surface where the vertical (or radial) motions are computed.

Treatment of Soil Response for Vertical Motions

Commonly, equivalent-linear site response analyses for vertical motions have used strain iterated shear moduli from a horizontal motion analysis to adjust the compression-wave velocities assuming either a strain independent Poisson's ratio or bulk modulus. Some fraction (generally 30% to 100%) of the strain iterated shear-wave damping is used to model the compression-wave damping and a linear analyses is performed for vertically propagating compression waves using the horizontal control motions scaled by some factor near 2/3.

The equivalent-linear approach implicity assumes some coupling between horizontal and vertical motions. This is necessitated by the lack of well determined M/M_{max} and damping curves for the constrained modulus. Ideally, the strain dependency of the constrained modulus should be determined independently of the shear modulus. Also, the conventional approach assumes vertically-propagating compression waves and not inclined P-SV waves. Additionally, the use of some fraction of the horizontal control motion is an approximation and does not reflect the generally greater high-frequency content of vertical component motions at rock sites due to lower kappa values (EPRI, 1993).

Alteratively, fully nonlinear analyses can be made using two- or three-component control motions (Costantino, 1967; 1969; Li et al., 1992; EPRI, 1993). These nonlinear analyses require two- or three-dimensional soil models which describe plastic flow and yielding and the accompanying volume changes as well as coupling between vertical and horizontal motions through Poisson's effect. While these analyses are important to examine expected dependencies of computed motions on material properties and may have applications to the study of soil compaction, deformation, slope stability, and component coupling, the models are very sophisticated and require specification of many parameters, at least some of which are poorly understood.

In the current implementation of the equivalent-linear approach to estimate vertical to horizontal response spectral ratios, the horizontal component analyses are performed for vertically propagating shear waves using an equivalent-linear random vibration theory (RVT) methodology coupled to the point-source stochastic ground motion model (EPRI, 1993; Schneider et al., 1993). To compute the vertical motions, a linear analysis is performed for incident inclined P-SV waves using low-strain, compression- and shear-wave velocities derived from the generic shear- and compression-wave velocity profiles (Figures 1 and 2). Compression-wave damping is assumed to be equal to the low strain shear-wave damping (Johnson and Silva, 1981). The horizontal component and vertical component analyses are assumed to be independent.

These approximations, linear analysis for the vertical component and uncoupled vertical and horizontal components, have been checked by comparing results of fully nonlinear analyses at soil sites Gilroy 2 and Treasure Island to recorded vertical and horizontal motions from the 1989 Loma Prieta earthquake (EPRI, 1993). The nonlinear analyses indicate that little coupling exists between the vertical and horizontal motions for the ranges in control motions analyzed (maximum about 0.5g). These assumptions are expected to result in conservative estimates of vertical motions since a

higher degree of coupling implies degradation of constrained modulus and an accompanying increase in compression-wave damping.

The point-source computational model has been validated for horizontal motions with the Loma Prieta earthquake by comparing recorded motions with model predictions (Schneider et al., 1995) and more recently with 14 additional earthquakes (**M** 5.0 - 7.4) at about 500 sites (BNL, 1997). For vertical motions, current validation includes comparisons of recorded motions to model predictions for the 1989 **M** 6.9 Loma Prieta earthquake (20 rock and 16 soil sites), 1992 **M** 7.2 Landers earthquake (3 rock and 9 soil sites), and the 1994 **M** 6.7 Northridge earthquake (16 rock and 56 soil sites). In general, vertical motions are not modeled as well as horizontal motions as the observed vertical motions show more variation than the horizontal and the model is not able to capture the increased variability. This is reflected in empirical relations as well, with a larger standard error associated with vertical motions (Abrahamson and Silva, 1997).

As an example of model predictions to recorded motions, Figure 28 shows recorded and computed vertical and horizontal motions for the **M** 7.2 Landers earthquake at the rock* site Lucerne ($D \approx 2$ km). The simple point-source, using the generic shallow rock profile with equivalent-linear analyses for the horizontal component and a linear analysis for the vertical appears to capture the general features of the recorded motions.

To generate V/H ratios based on numerical modeling, the shallow generic profiles (Figures 1 and 2) were placed on top of the generic California crust (Figure 31). For equivalent-linear analyses, recently developed rock and cohesionless soil G/G_{max} and hysteretic damping curves (BNL, 1997) were used. The point-source stress drop was 60 bars, based on inversions of the Abrahamson and Silva (1997) empirical attenuation (BNL, 1997), and the source depth is taken as 8 km (the same as in the inversions).

To compare simulated V/H ratios to the empirical, Figures 29 and 30 show results for rock and soil sites for **M** 6.5, the best constrained magnitude for the empirical relations. In general the model captures the overall shapes and trends with distance of the empirical ratios but shows a stronger close-in distance effect. This strong distance effect is controlled by the incidence angle (top of source layer) increasing rapidly with increasing epicentral distance. As previously mentioned, crustal heterogeneity as well as source finiteness would tend to weaken this distance dependence. For the point-source model, crustal randomization to simulate uncertainty and randomness in the crustal structure would reduce the near-source distance dependency making it similar to the empirical. However, the simple point-source model, as implemented here, captures the general trends of the WUS empirical rock and soil V/H ratios well enough to provide guidance in assessing the appropriateness of applying WUS ratios to CEUS conditions.

To generate V/H ratios for the CEUS, a generic midcontinent crustal model is used (EPRI, 1993). The CEUS crustal model is considered appropriate for hard rock sites in the CEUS east of the Rocky Mountains with the possible exception of the Gulf Coast region. This region has a crustal structure somewhat intermediate between the WUS and the CEUS (EPRI, 1993). The large difference

*The Lucerne site is actually a shallow (15 ft) soil over very hard rock (unweathered granite).

between the two generic crustal models shown in Figure 31 gives rise to significantly different short-period strong ground motion characteristics at close-in distances (as depicted in Figure 24) as well as different rates of attenuation with distance. These differences may be expected to impact the V/H ratios as well. For the WUS ratios, both the empirical and numerical model results showed that the stiffer profile (rock verses soil) resulted in lower short period ($\leq$ 0.3 sec) V/H ratios but larger long period ratios. For the hard rock CEUS crust, this trend may be expected to continue resulting in a lower maximum V/H ratio with perhaps a higher long period level. Due to the lower horizontal and vertical kappa values for the CEUS crust, the peak in the V/H ratio may be expected to occur at much shorter periods than in the CEUS rock ratios. These expected trends are reflected in the model prediction shown in Figure 32 (top plot). For CEUS hard rock sites, the peak V/H ratio is significantly lower and at a shorter period than soft rock sites and the long period level is higher as well. This difference between WUS and CEUS in the period range of 0.1 to 1.0 sec was also found by Atkinson and Boore (1997) in an empirical analysis of the H/V ratio of Fourier amplitude spectra at large distances ($D \geq 20$ km) in Western and Eastern Canada.

For deep soil sites, Figure 32 (bottom) plot) suggests that the V/H ratio may be significantly higher in the CEUS than in WUS. This result is primarily due to nonlinear soil response in the horizontal component as well as assuming linear response for the verticals. The factors contributing to the higher degree of nonlinear response for the CEUS soil ratios are the higher levels of high frequency energy in the control motions (Figure 24), the larger overall motions due to the higher stress drop (100 bars for CEUS and 60 bars for WUS), and the large jump in shear-wave velocity in going from the base of the soil to the top layer of the CEUS crust (Figure 31). These results suggest that for both rock and soil CEUS V/H ratios, it is probably inappropriate to adopt WUS ratios for design purposes. A similar conclusion was reached in the EPRI (1993) project to estimate strong ground motion in the CEUS. In that project, design V/H ratios were developed for CEUS rock and stiff soil conditions based primarily on model simulations.

It should be emphasized that only a single and very simple model, which involves many assumptions, has been implemented here. However, the results may provide a useful contribution to developing design V/H ratios for CEUS conditions. Naturally, the most satisfying approach is to make use of multiple well validated models to assess the range in uncertainty in the CEUS V/H ratios.

Conclusions

Characteristics of vertical and horizontal component strong ground motions have been examined to reveal general trends which may be of significance to structural analyses. Recordings at both rock and deep soil sites representative of WUS showed distinctly different behavior of vertical motions at rock and soil sites at close source distances ($D \leq$ 10 to 15 km). At rock sites, the largest motions tend to occur on all three components at nearly the same time and "in-phase" motion is present on acceleration, velocity, and displacement time histories. Vertical component response spectra can exceed those of the horizontal components at short periods ($T \leq 0.1$ sec) by moderate amounts (20% on average) and at very close fault distances ($D \leq 5$ km).

At soil sites, short period ($T \leq 0.2$ sec) vertical motions, as revealed by acceleration time histories, occur "out-of-phase" with the largest motions on the horizontal components. For intermediate-to-

long periods, however, near-source soil site velocity and displacement time histories are "in-phase", showing the dominant motion occurring at about the same time. At close source distances ($D \leq 5$ km) short period ($T \leq 0.1$ sec) vertical motions may exceed horizontal motions by a factor of 2.

Analyses of vertical and horizontal component statistical response spectral shapes for both rock and soil sites at varying magnitudes and distances showed significantly less damping at both rock and soil sites for vertical motions. These analyses also suggested that vertical motions are largely linear at both rock and soil sites. Horizontal motions, on the other hand, for earthquakes of **M** 6.0 to 7.0+ and at source distances within 10 km showed a broad-band shift in spectral shape to longer periods consistent with an increase in damping due to nonlinear site response.

Response spectral ratios (V/H) were computed from median WUS empirical horizontal and vertical component response spectra at rock and soil sites for a suite of distances (Figure 26). These empirical V/H ratios may be used to obtain ratios for applications to structural design for WUS conditions.

Nonlinear response in horizontal motions coupled with largely linear response for vertical motions at soil sites is expected to result in larger V/H ratios for soil sites compared to rock sites at close distances as well as a stronger magnitude dependency. This trend is seen in V/H ratios computed using empirical attenuation relations and at least a portion of these dependencies is attributed to nonlinear response involving horizontal motions at soil sites.

To estimate V/H ratios for CEUS hard rock and deep soil conditions, a simple point-source model is used to predict both rock and soil horizontal and vertical motions. The model treats vertical motions as inclined P-SV waves with a linear analysis and horizontal motions as vertically incident shear-waves using equivalent-linear analyses. Model predictions for WUS V/H ratios showed generally favorable agreement with empirical V/H ratios. Application of the simple model to CEUS showed generally higher V/H ratios for hard rock sites compared to soft rock sites at long periods ($T > 0.3$ sec). At short periods, the peak in the V/H ratio is shifted from about 0.07 sec for soft rock to about 0.013 sec for hard rock. These results are due to the lower shallow crustal damping at the hard rock site.

For soil sites, the CEUS V/H ratio is predicted to be significantly larger than the corresponding WUS ratio. This is attributed to higher levels of nonlinear soil response on the horizontal motions due to CEUS rock control motions richer in short period energy, higher overall levels of control motions due to higher CEUS stress drops (100 bars compared to 60 bars), and a larger impedance contrast at the base of the soil column. Due to the simplicity of the model and the number of significant assumptions, use of multiple well validated models is recommended in developing design V/H ratios for the CEUS.

In general, the conventional V/H factor of 2/3 is probably not appropriate at CEUS rock and soil sites and may only be appropriate for WUS sites at periods beyond about 0.3 sec and for distances beyond about 50 km.

REFERENCES

Abrahamson, N.A. and Silva, W.J. (1997). "Empirical response spectral attenuation relations for shallow crustal earthquakes." *Seism. Soc. Am.,* 68(1), 94-127.

Anderson, J.G. (1991). "A preliminary descriptive model for the distance dependence of the spectral decay parameter in southern California." *Bull. Seism. Soc. Am.,* 81(6), 2186-2193.

Anderson, J. G. and S. E. Hough (1984). "A Model for the Shape of the Fourier Amplitude Spectrum of Acceleration at High Frequencies." *Bull. Seism. Soc. Am.,* 74(5), 1969-1993.

Atkinson, G.M. and Boore, D.M. (1997). "Some comparisons between recent ground-motion relations." *Seism. Res. Lett.* 68(1), 24-40.

Bozorgina, Y., M. Niazi, and K.W. Campbell (1995). "Characteristics of free-field vertical ground motion during the Northridge earthquake." *Earthquake Spectra,* 11(4), 515-525.

Bozorgina, Y. and M. Niazi (1993). "Distance scaling of vertical and horizontal response spectra of the Loma Prieta earthquake." *Earthquake Engineering and Soil Dynamics,* 22, 695-707.

Brookhaven National Laboratory (1997). "Description and validation of the stochastic ground motion model." Submitted to Brookhaven National Laboratory, Associated Universities, Inc. Upton, New York.

Chang, S.W., J.D. Bray and R.B. Seed (1996). "Engineering implications of ground motions from the Northridge earthquake." *Bull. Seism. Soc. Am.,* 86(1B), S270-S288.

Electric Power Research Institute (1993). "Guidelines for determining design basis ground motions." Palo Alto, Calif: Electric Power Research Institute, vol. 1-5, EPRI TR-102293.

Niazi, M. and Y. Bozorgnia (1991). "Behavior of near-source peak horizontal and vertical ground motions over smart-1, array, Taiwan." *Bull. Seism. Soc. Am.,* 81(3), 715-732.

Newmark, N.M. and W.J. Hall (1978). "Development of criteria for seismic review of selected nuclear power plants." NUREG/CR-0098, Nuclear Regulatory Commission.

Kawase, H. and K. Aki (1990). "Topography effect at the critical SV-wave incidence: possible explanation of damage pattern by the Whittier Narrows, California, earthquake of 1 October 1987." *Bull. Seism. Soc. Am.,* 80(1), 1-30.

Sadigh, C.-Y. Chang, J.A. Egan, F. Makdisi, and R.R. Youngs (1997). "Attenuation relationships for shallow crustal earthquakes based on California strong motion data." *Seism. Soc. Am.,* 68(1), 180-189.

Schneider, J.F., W.J. Silva, and C.L. Stark (1993). "Ground motion model for the 1989 **M** 6.9 Loma Prieta earthquake including effects of source, path and site." *Earthquake Spectra,*

9(2), 251-287.

Silva, W.J. and R. Darragh (1995). "Engineering characterization of earthquake strong ground motion recorded at rock sites." Palo Alto, Calif:Electric Power Research Institute, TR-102261.

Silva, W.J. (1976). "Body Waves in a Layered Anelastic soilid." *Bull. Seis. Soc. Am.*, 66(5), 1539-1554.

Wald, D.J., Heaton, T.H. (1994). "Spatial and temporal distribution of slip for the 1992 Landers, California, earthquake." *Bull. Seism. Soc. Amer.*, 84(3), 668-691.

Table 1

GEOMATRIX CONSULTANTS

STRONG-MOTION RECORDING STATIONS
CLASSIFICATION SYSTEM

Geotechnical Subsurface Characteristics

Designation	Description
A	Rock. Instrument is founded on rock material (V_S > 600 mps (1969 ft/sec) or a very thin veneer (less than 5m (16 ft)) of soil overlying rock material.
B	Shallow (stiff) soil. Instrument is founded in/on a soil profile up to 20m (66 ft) thick overlying rock material, typically in a narrow canyon, near a valley edge, or on a hillside.
C	Deep narrow soil. Instrument is founded in/on a soil profile at least 20m (66 ft) thick overlying rock material in a narrow canyon or valley no more than several kilometers wide.
D	Deep broad soil. Instrument is founded in/on a soil profile at least 20m (66 ft) thick overlying rock material in a broad canyon or valley.
E	Soft deep soil. Instrument is founded in/on a deep soil profile that exhibits low average shear-wave velocity (V_S < 150 mps (492 ft/sec)).

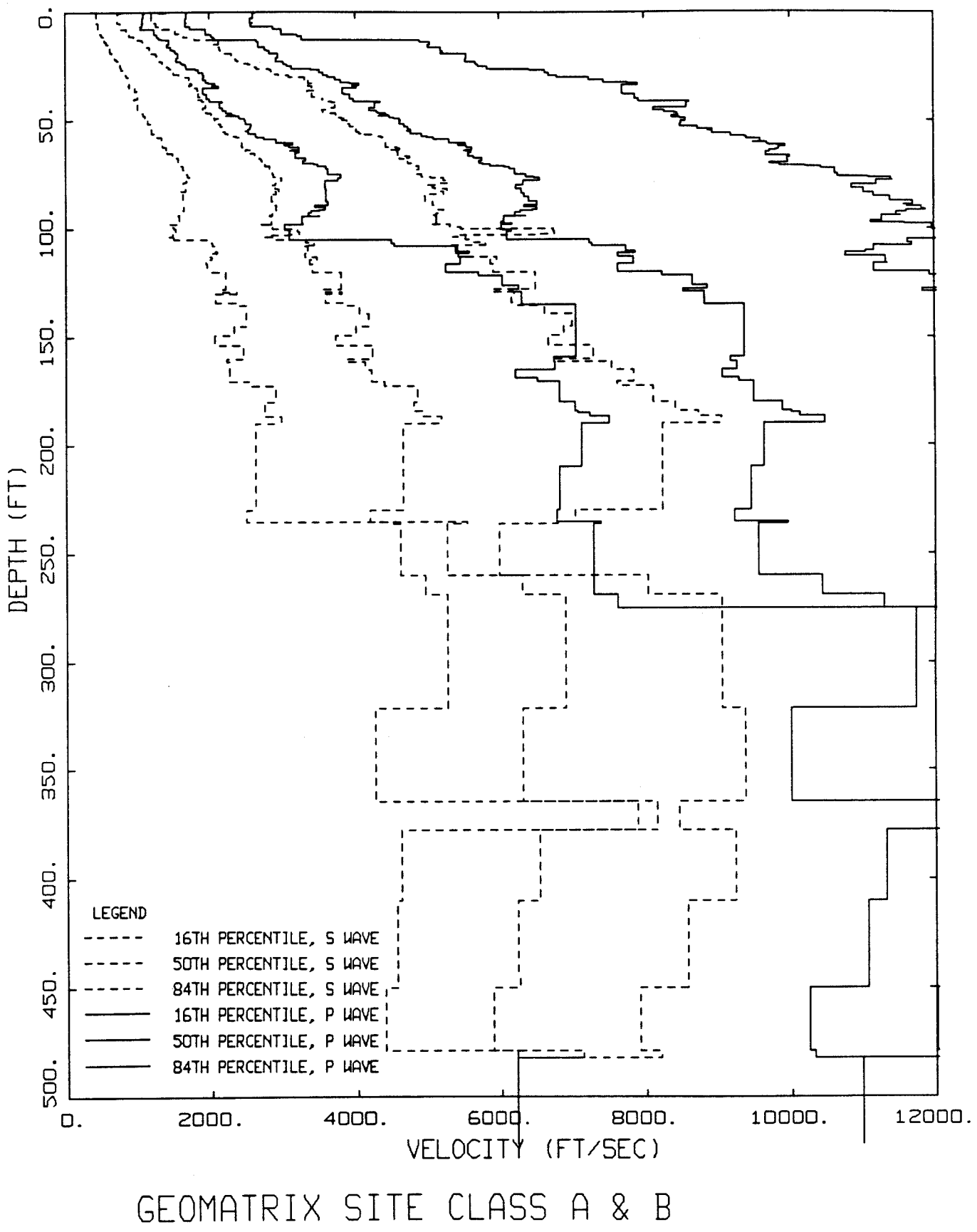

Figure 1. Median and $\pm$ 1 σ compression- and shear-wave velocity profiles for Geomatrix site class A plus B (soft rock, Table 1).

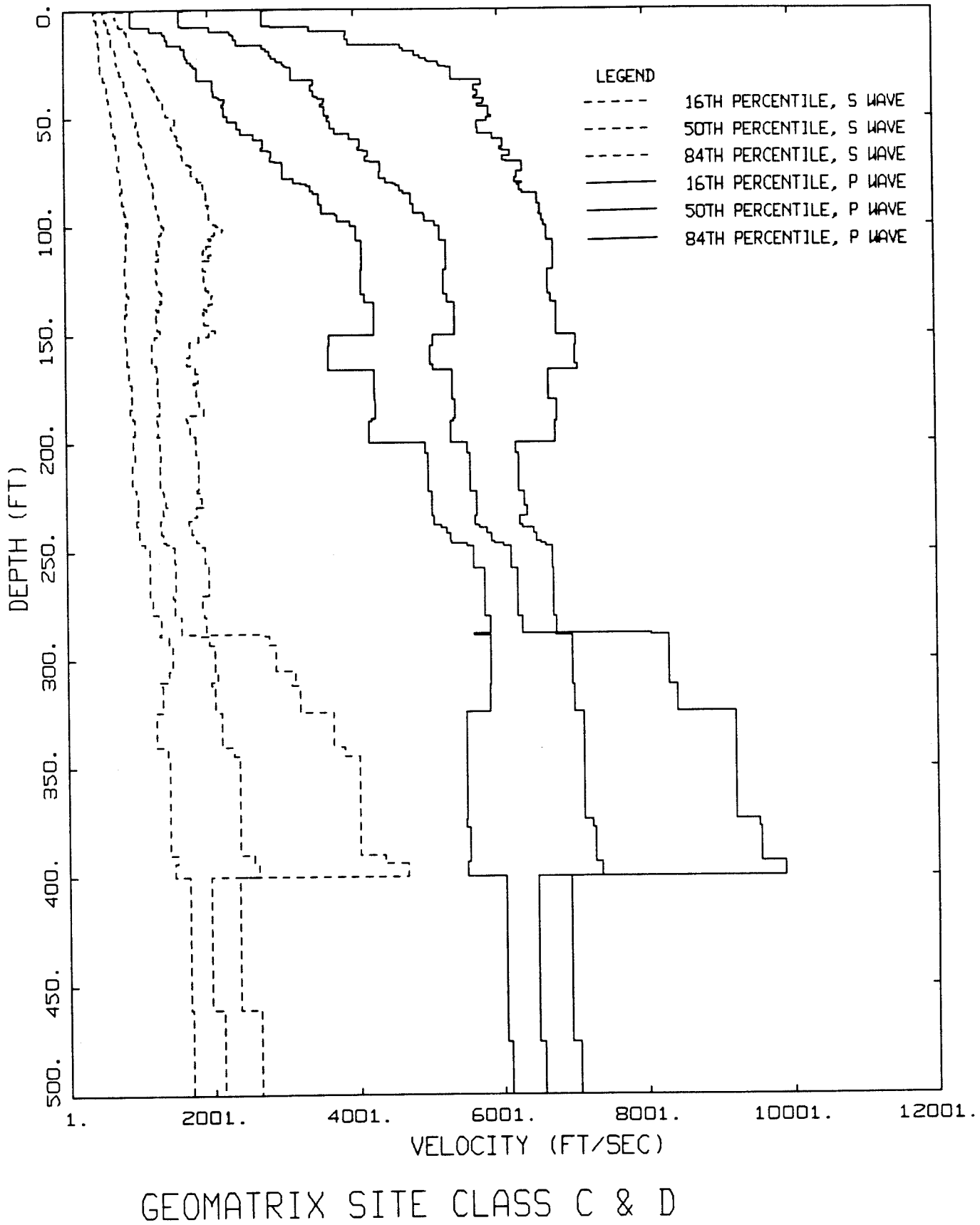

Figure 2. Median and $\pm$ 1 σ compression- and shear-wave velocity profiles for Geomatrix site class C plus D (deep soil, Table 1).

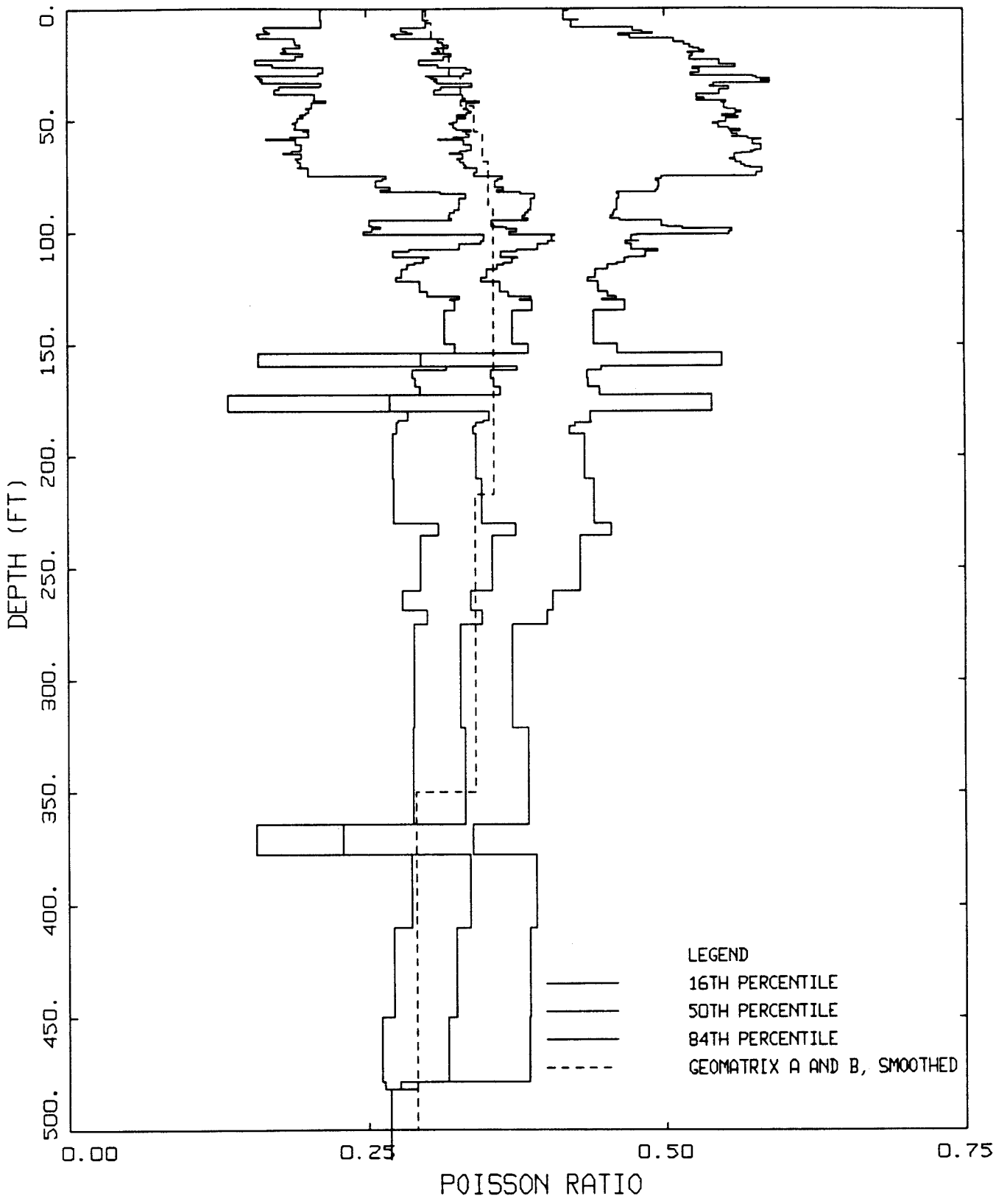

Figure 3. Median and $\pm$ 1 σ Poisson's ratio profiles for Geomatrix site class A plus B (soft rock, Table 1).

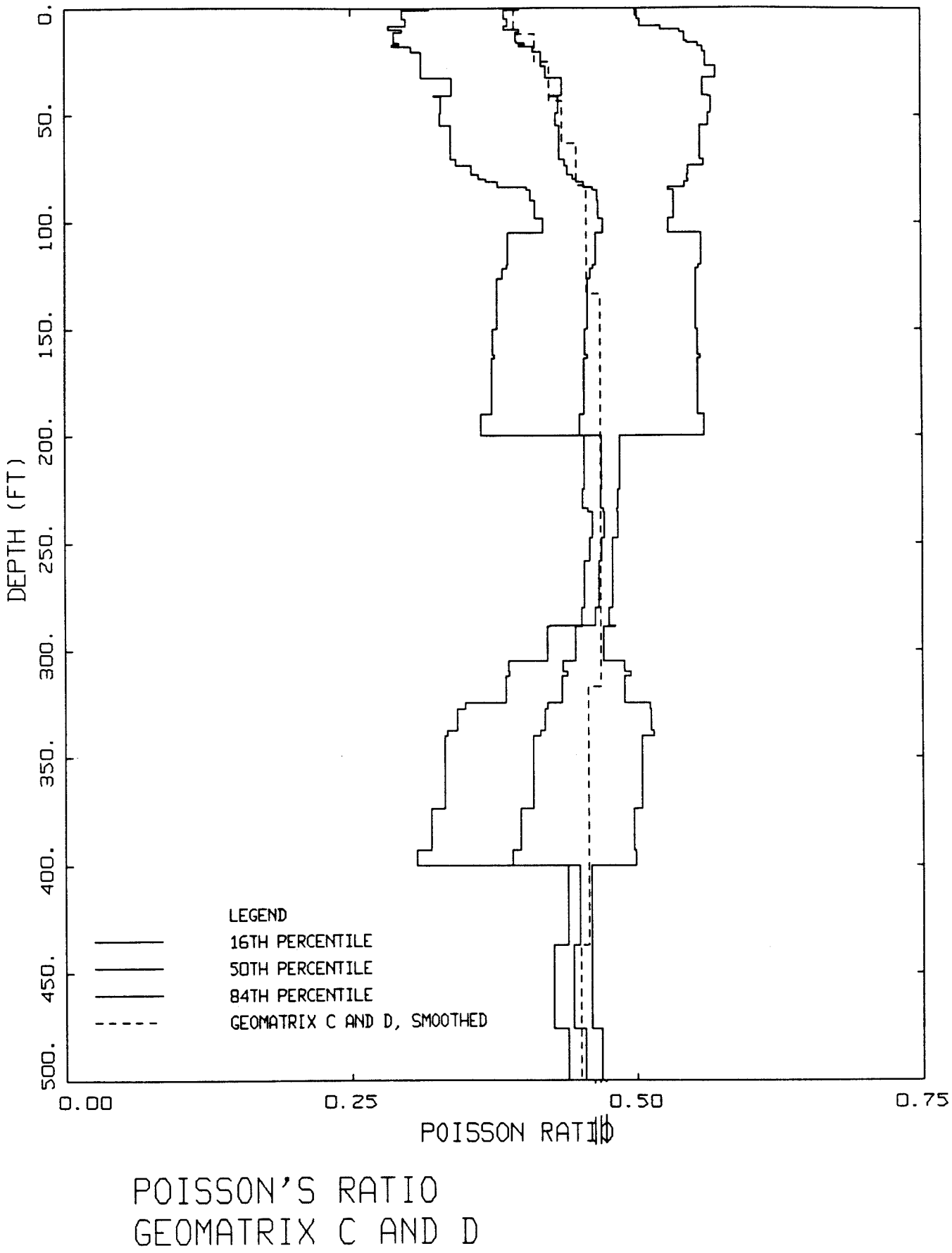

Figure 4. Median and $\pm$ 1 σ Poisson's ratio profiles for Geomatrix site class C plus D (deep soil, Table 1).

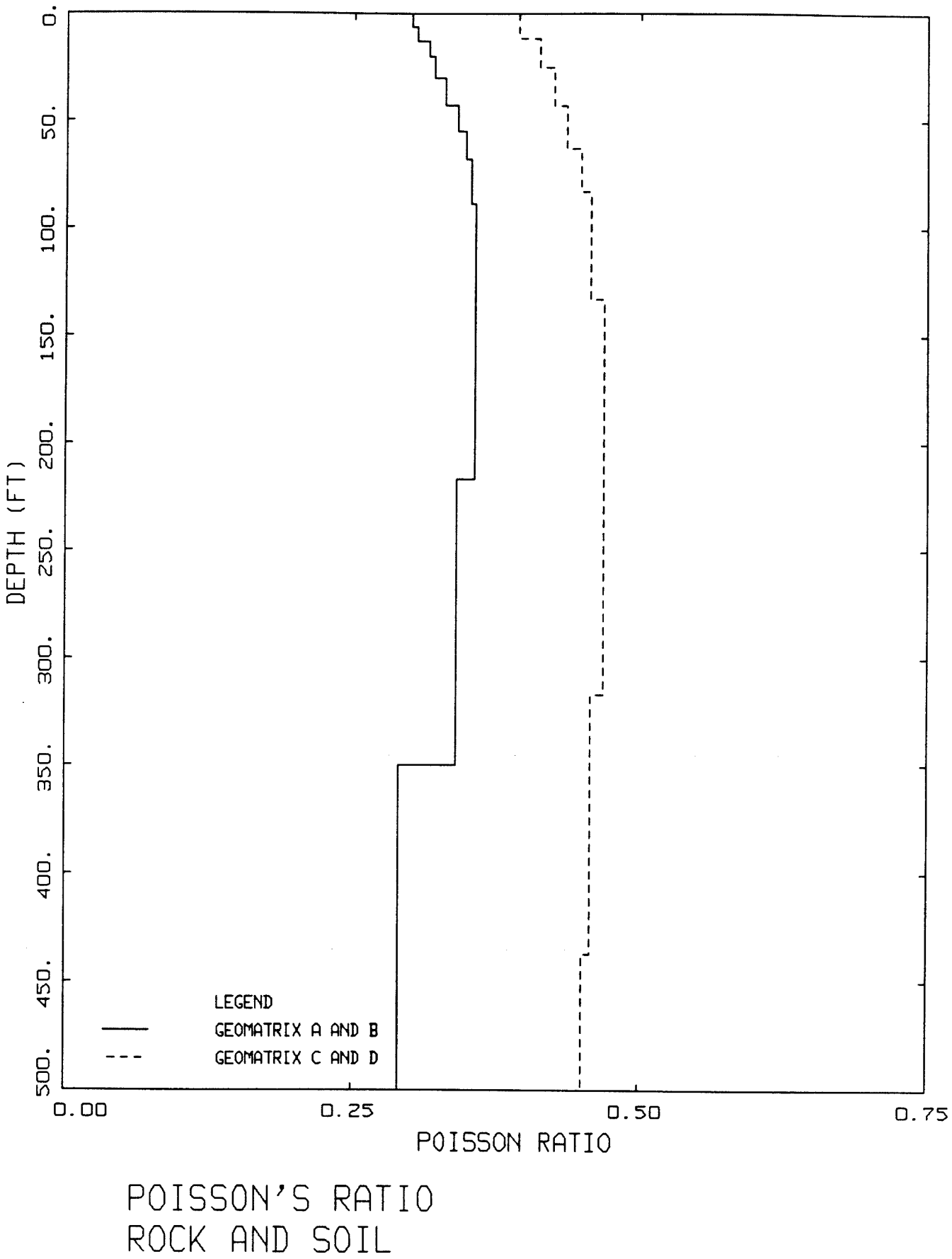

Figure 5. Poisson's ratio models for Geomatrix site classes A plus B and C plus D (Table 1).

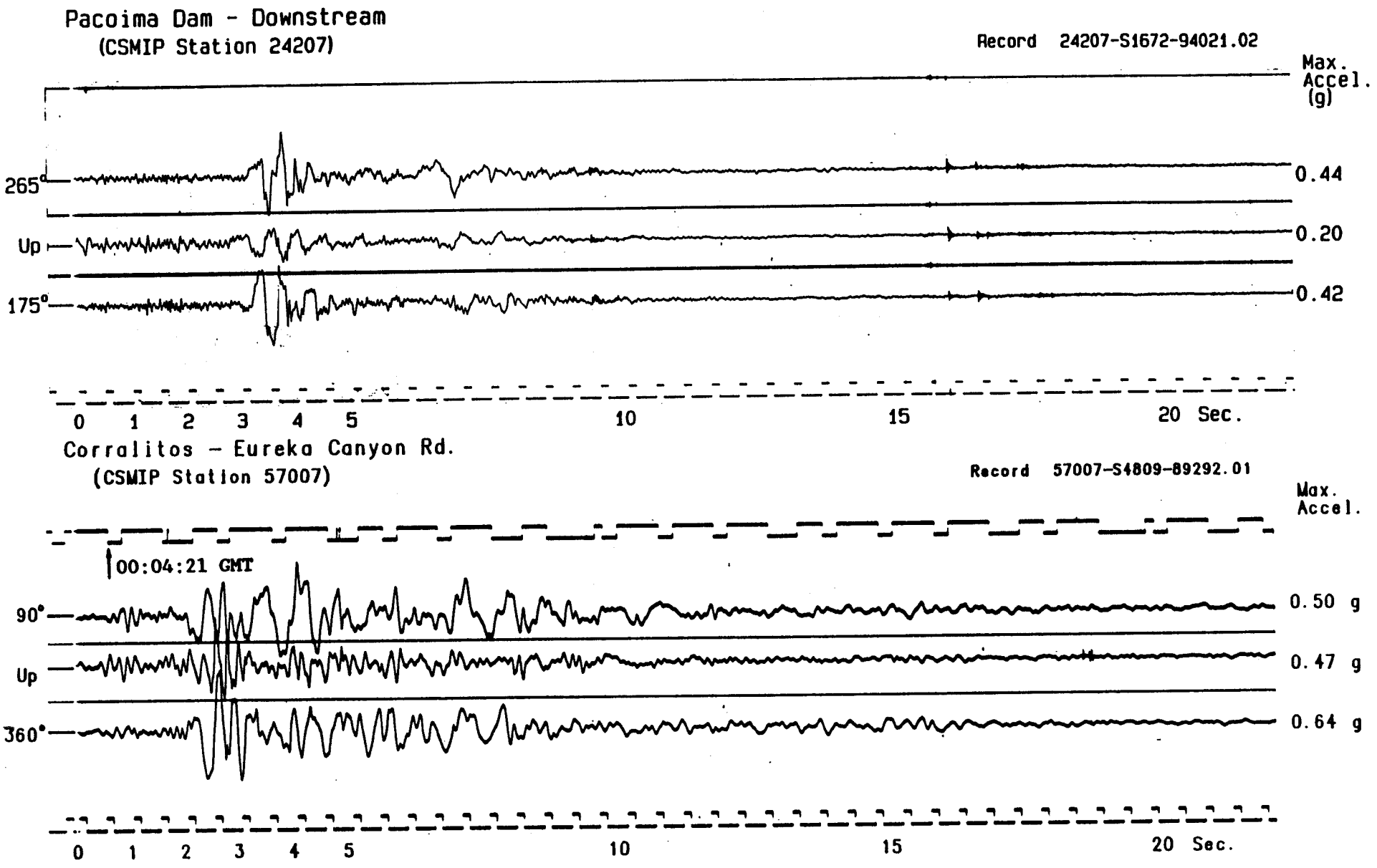

Figure 6. Horizontal and vertical component acceleration time histories recorded at rock sites Pacoima Downstream for the 1994 M 6.7 Northridge earthquake (top) and Corralitos for the 1989 M 6.9 Loma Prieta earthquake (bottom). (Source: CDMG initial data reports).

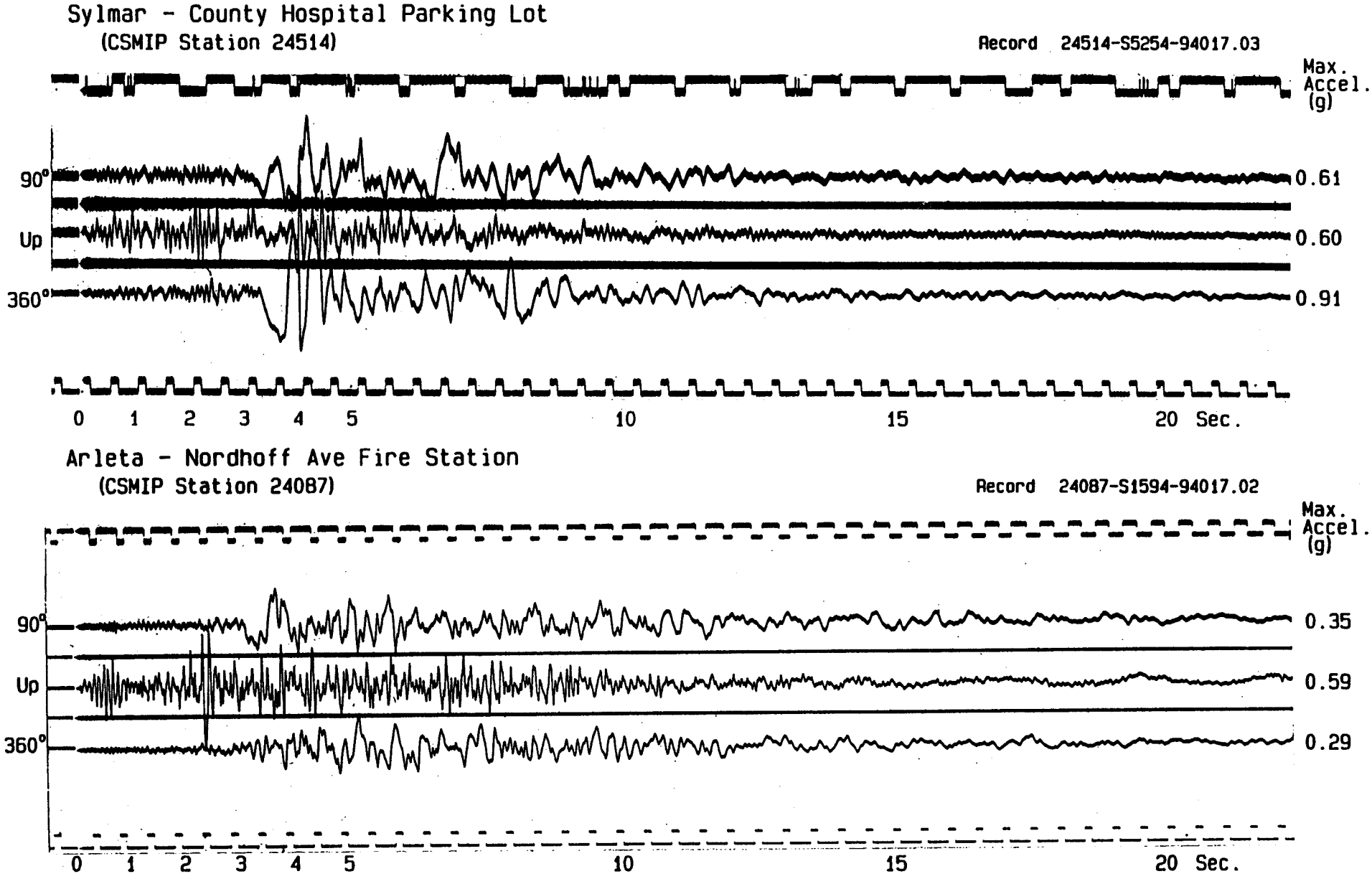

Figure 7. Horizontal and vertical component acceleration time histories recorded at soil sites Sylmar (top) and Arleta (bottom) for the 1994 M 6.7 Northridge earthquake. (Source: CDMG initial data reports).

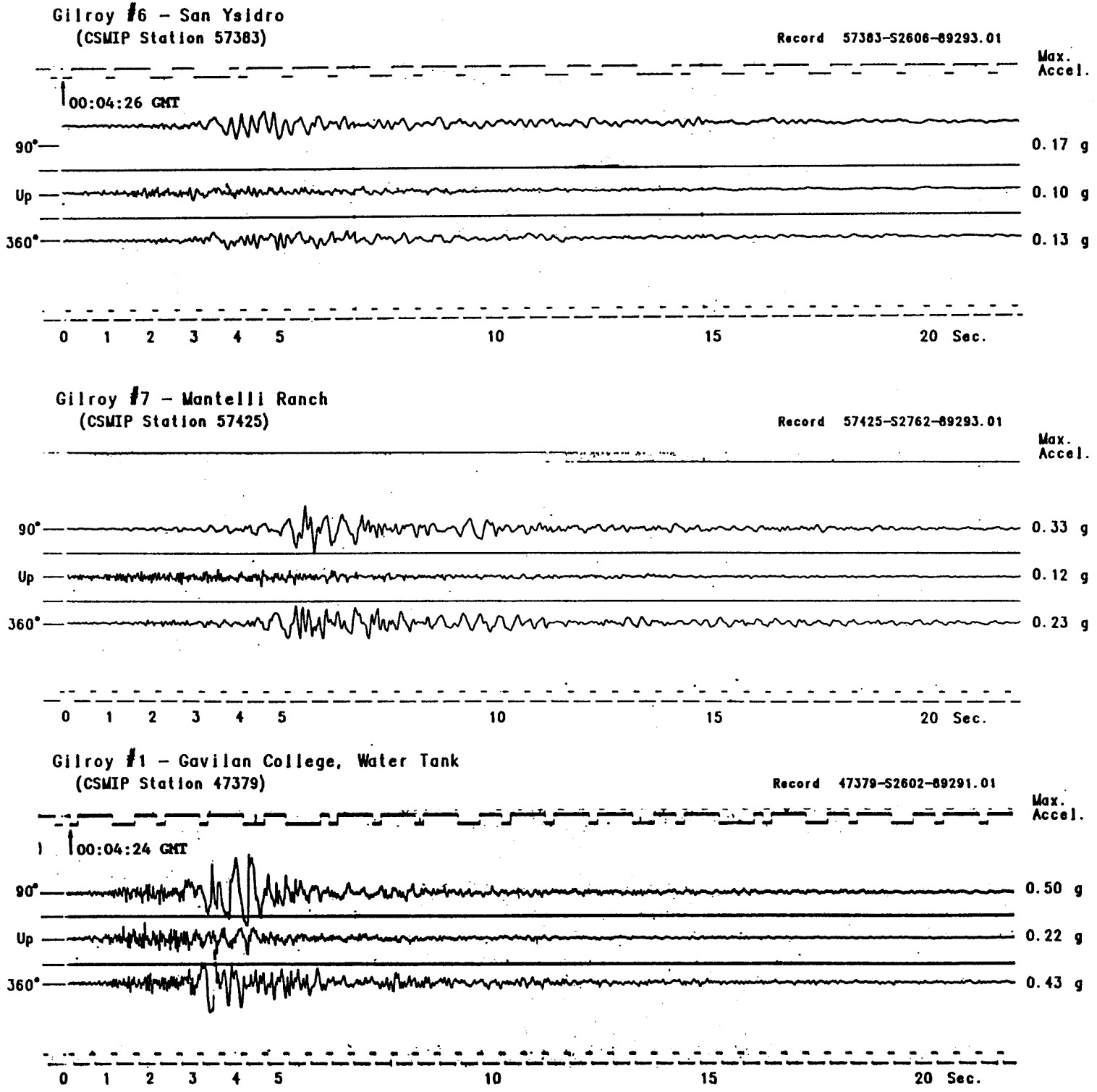

Figure 8. Horizontal and vertical component acceleration time histories recorded at rock sites Gilroy 6, 7, and 1 (top, middle, and bottom) for the 1989 M 6.9 Loma Prieta earthquake. (Source: CDMG initial data reports).

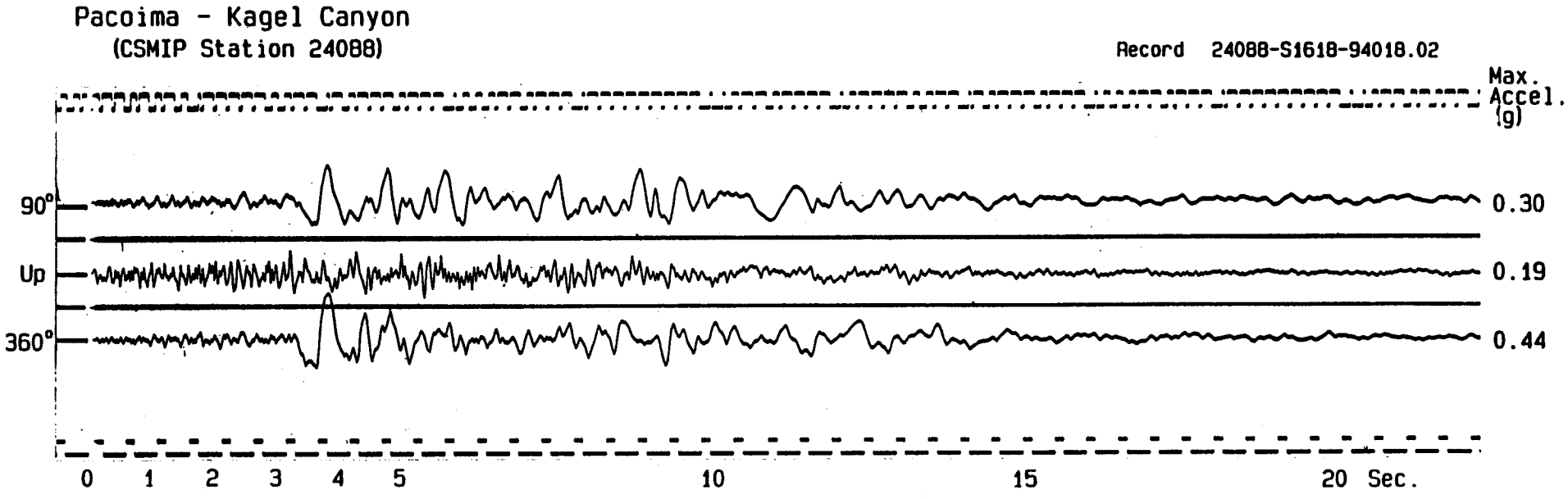

Figure 9. Horizontal and vertical component acceleration time histories recorded at "rock" site Pacoima Kagel for the 1994 M 6.7 Northridge earthquake. (Source: CDMG initial data reports).

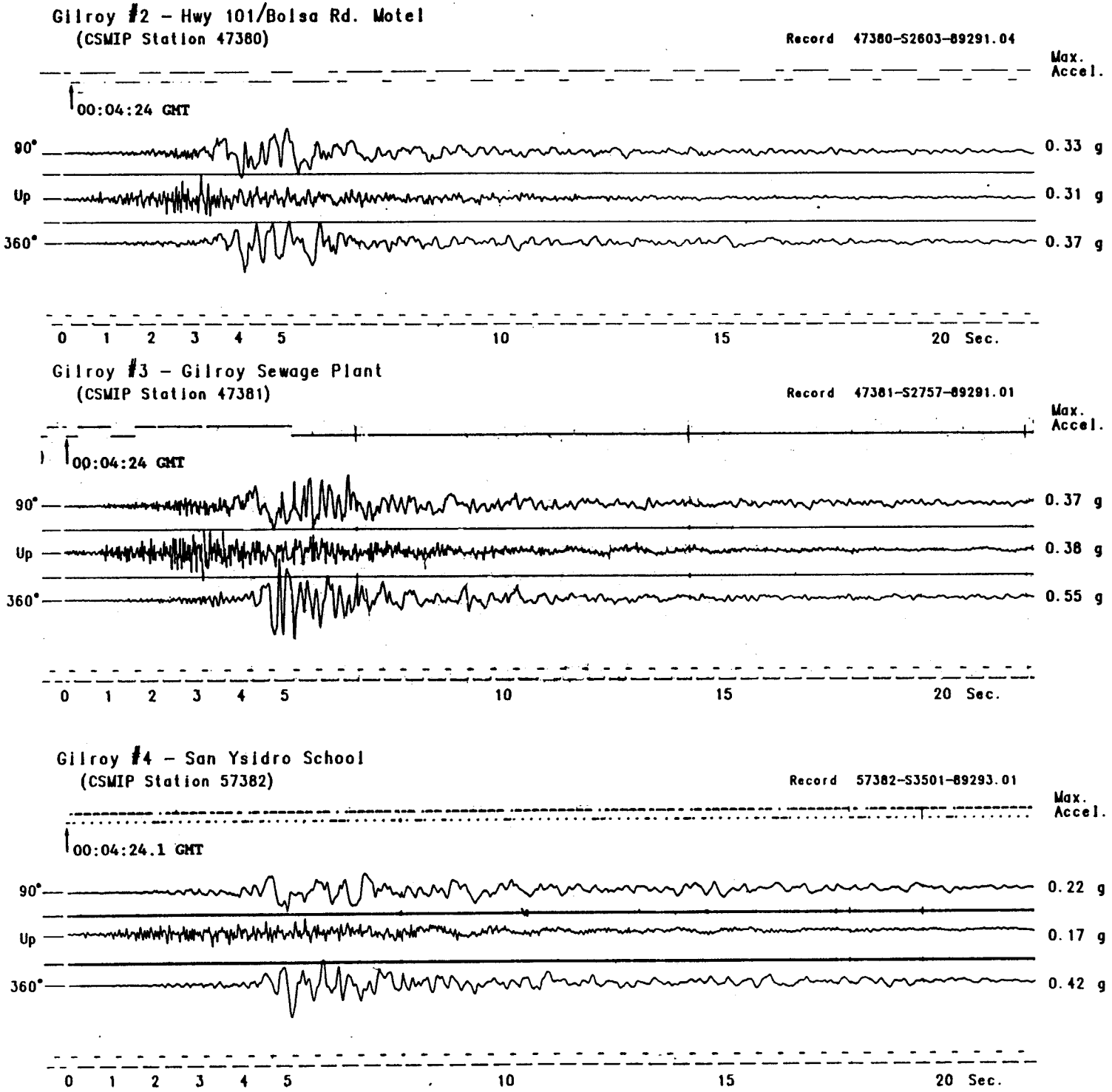

Figure 10. Horizontal and vertical component acceleration time histories recorded at soil sites Gilroy 2, 3, and 4 (top, middle, and bottom) for the 1989 M 6.9 Loma Prieta earthquake. (Source: CDMG initial data reports).

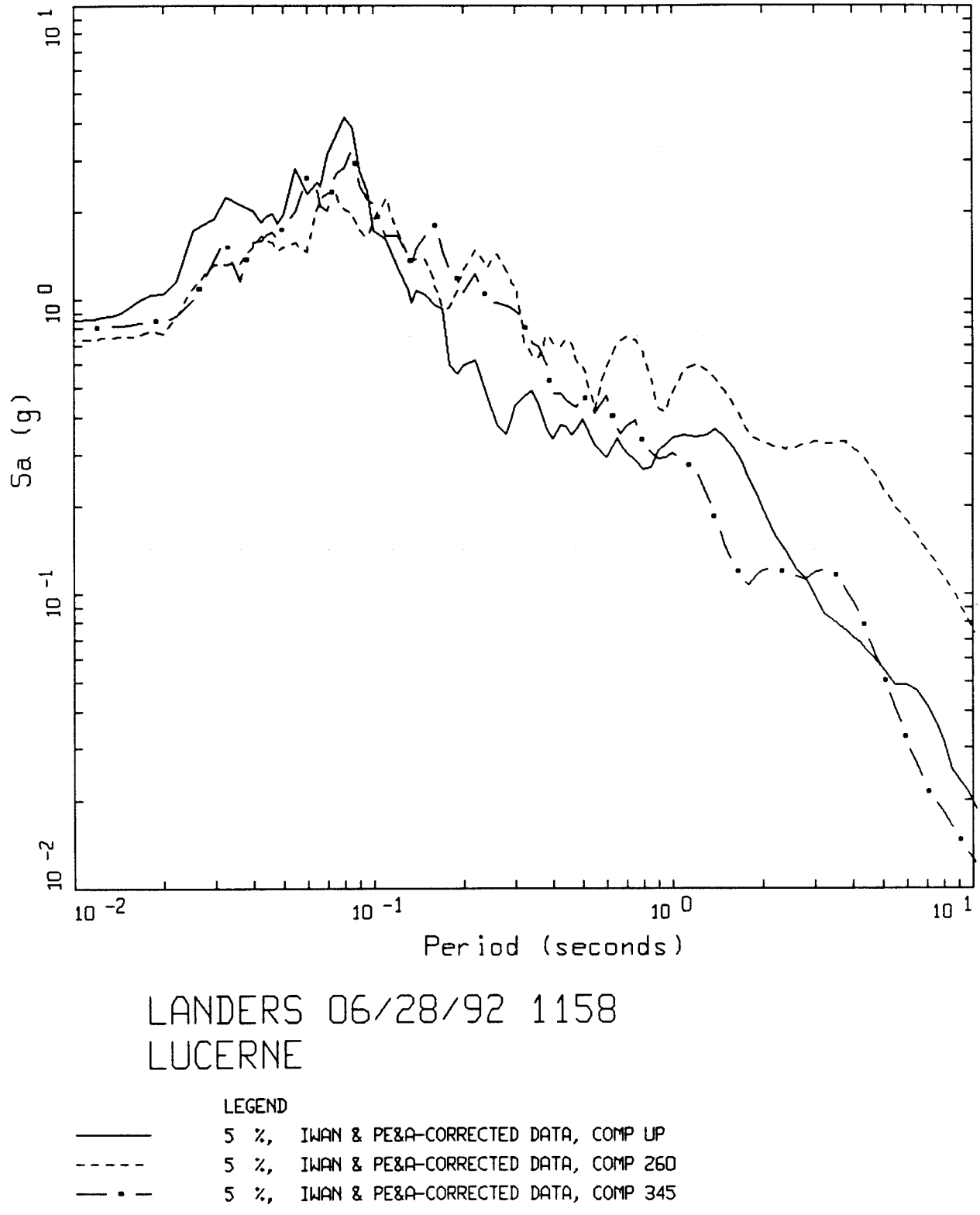

Figure 11. 5% Damped pseudo absolute response spectra at the SCE rock site Lucerne for the 1992 M 7.2 Landers earthquake. Fault distance is about 2 km.

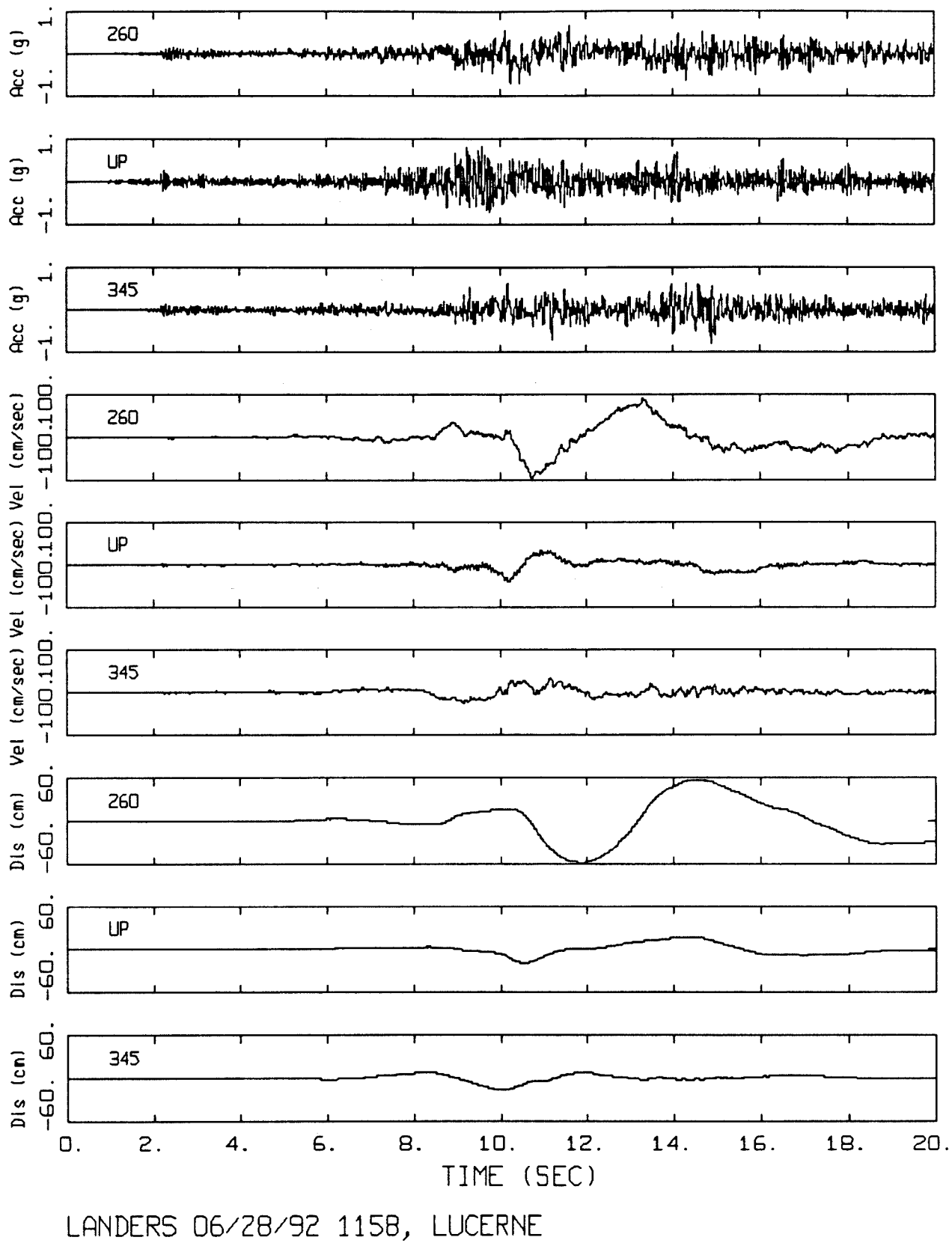

Figure 12. Acceleration, velocity, and displacement time histories at the SCE rock site Lucerne for the 1992 **M** 7.2 Landers earthquake. Fault distance is about 2 km.

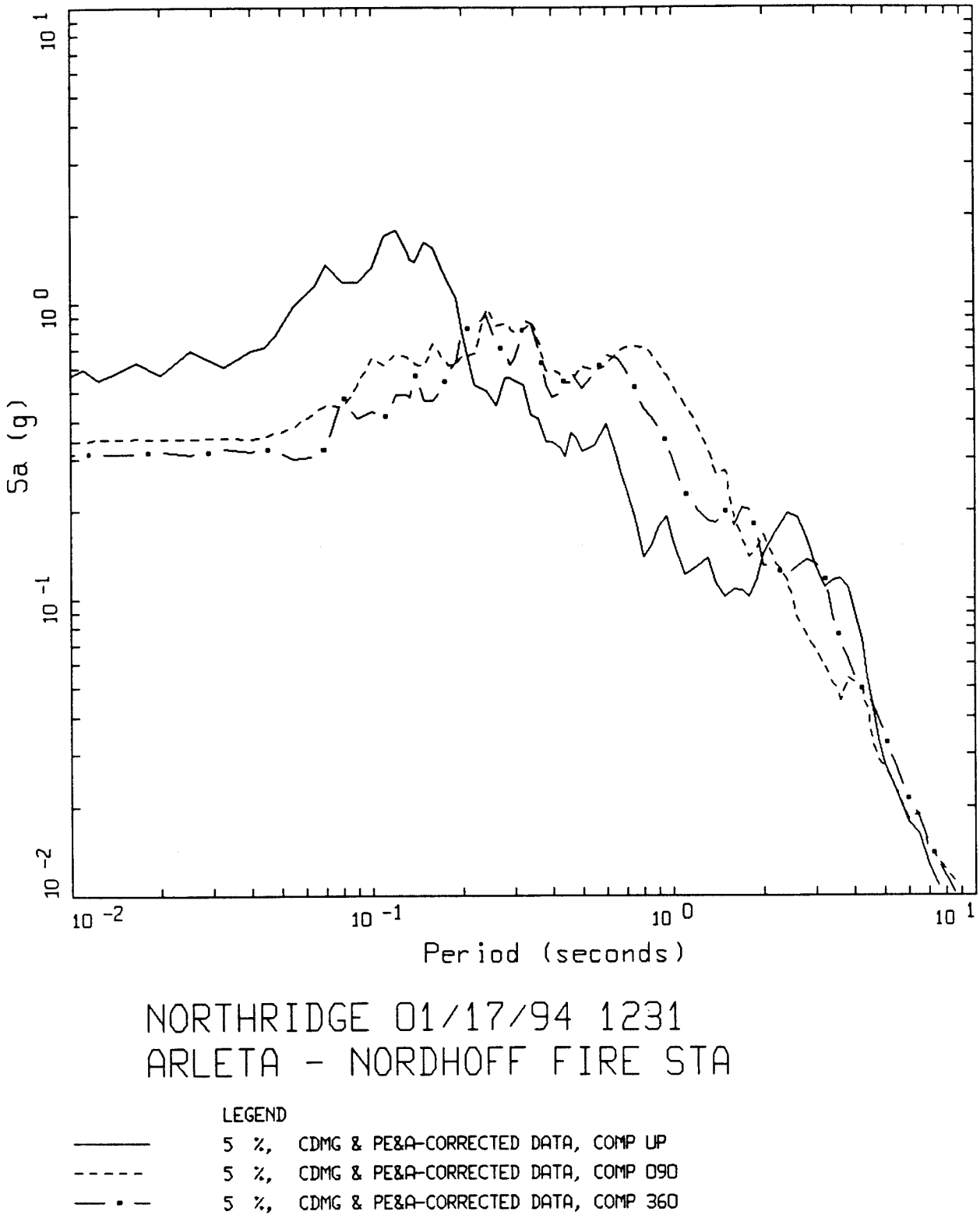

Figure 13. 5% Damped pseudo absolute response spectra at the soil site Arleta for the 1994 M 6.7 Northridge earthquake. Fault distance is about 9 km.

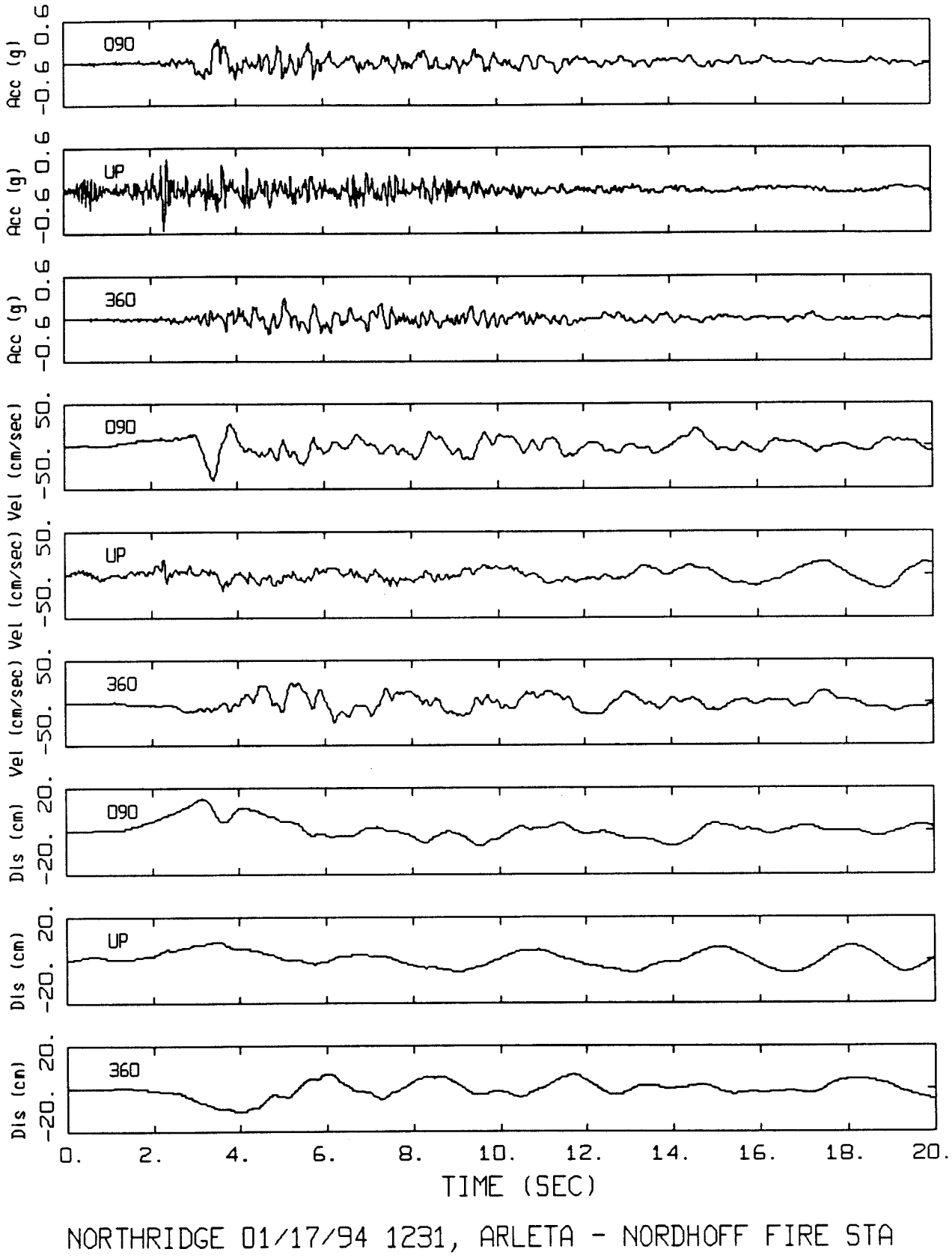

Figure 14. Acceleration, velocity, and displacement time histories at the soil site Arleta for the 1994 **M** 6.7 Northridge earthquake. Fault distance is about 9 km.

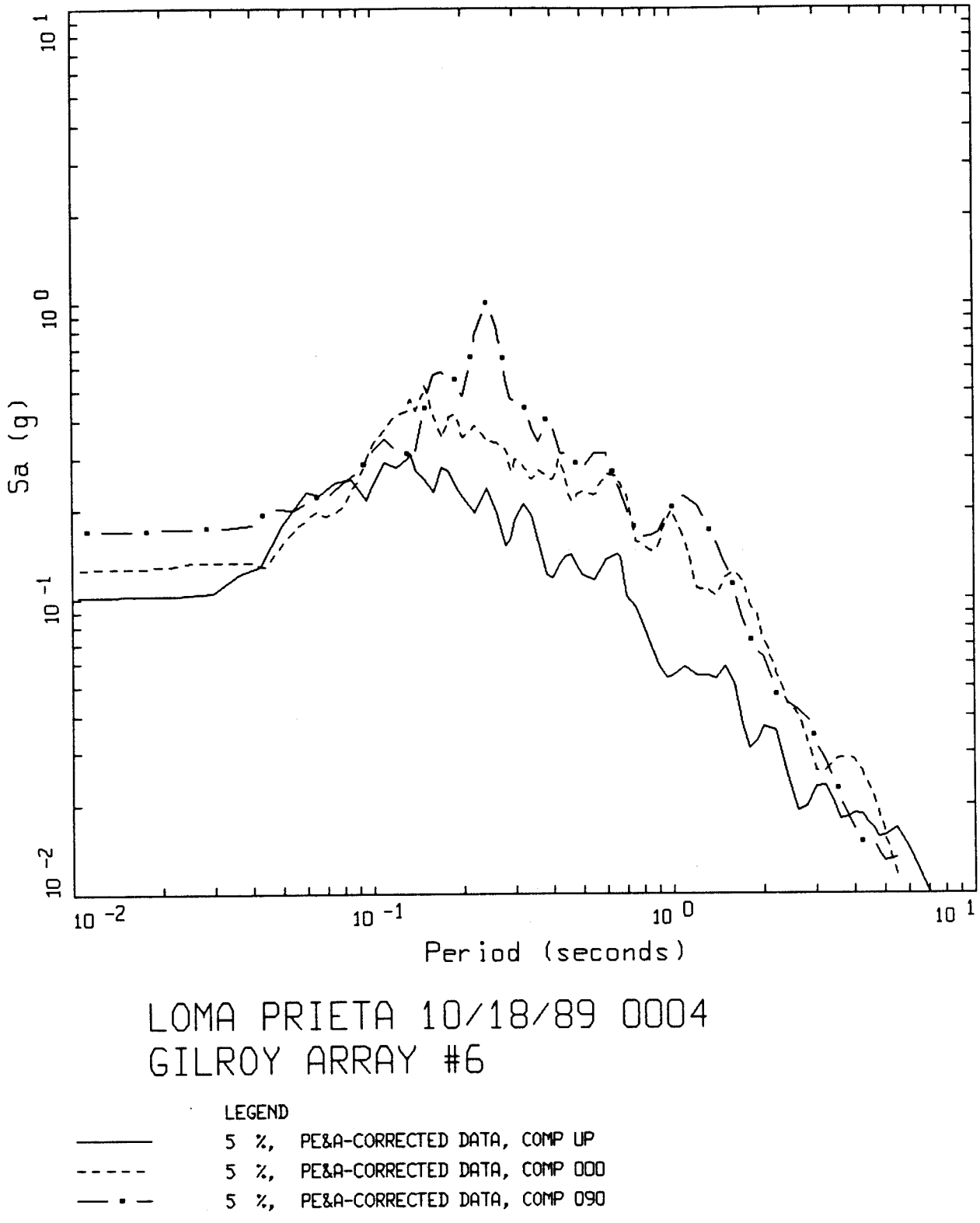

Figure 15. 5% Damped pseudo absolute response spectra at the rock site Gilroy 6 for the 1989 M 6.9 Loma Prieta earthquake. Fault distance is about 19 km.

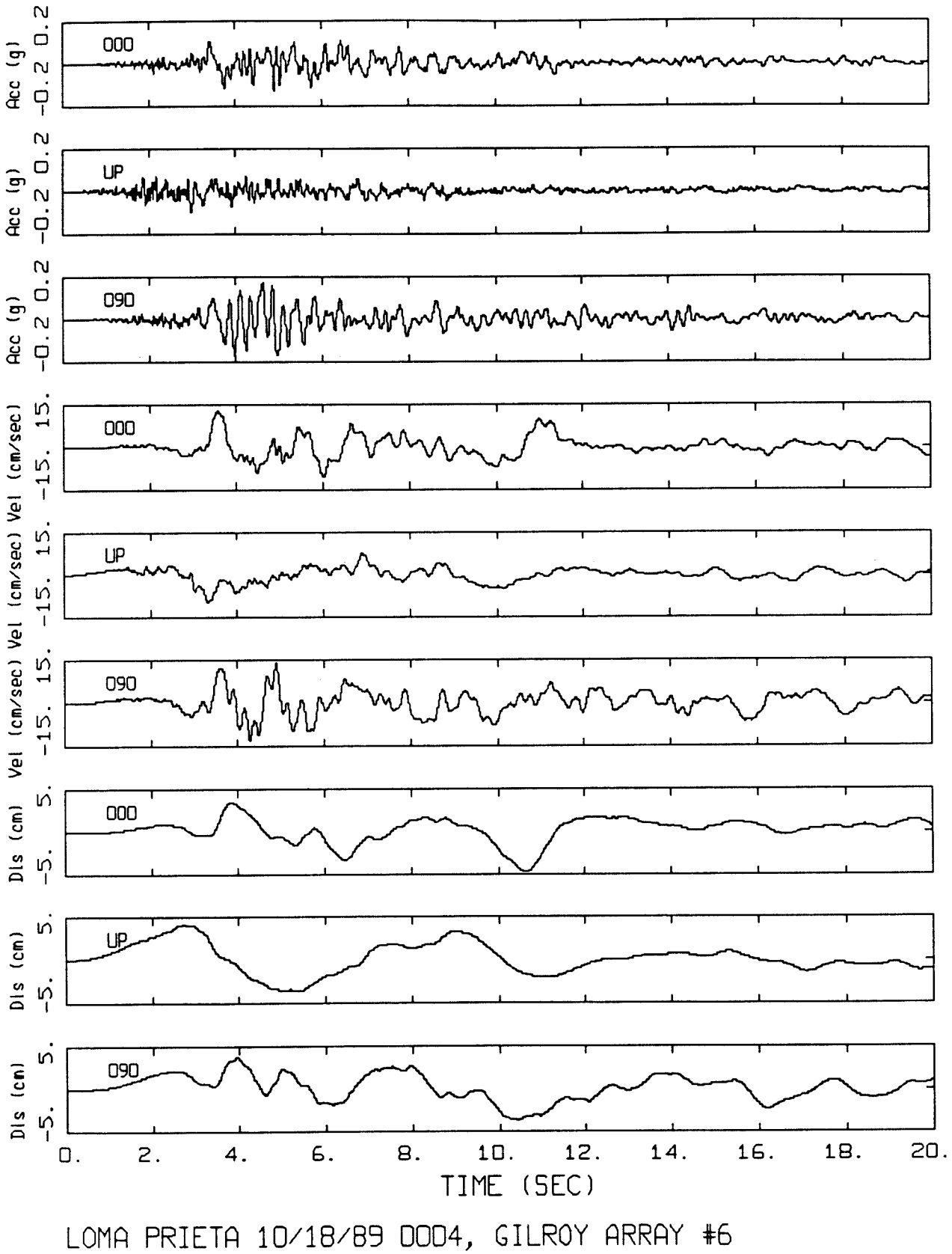

Figure 16. Acceleration, velocity, and displacement time histories at the rock site Gilroy 6 for the 1989 M 6.9 Loma Prieta earthquake. Fault distance is about 19 km.

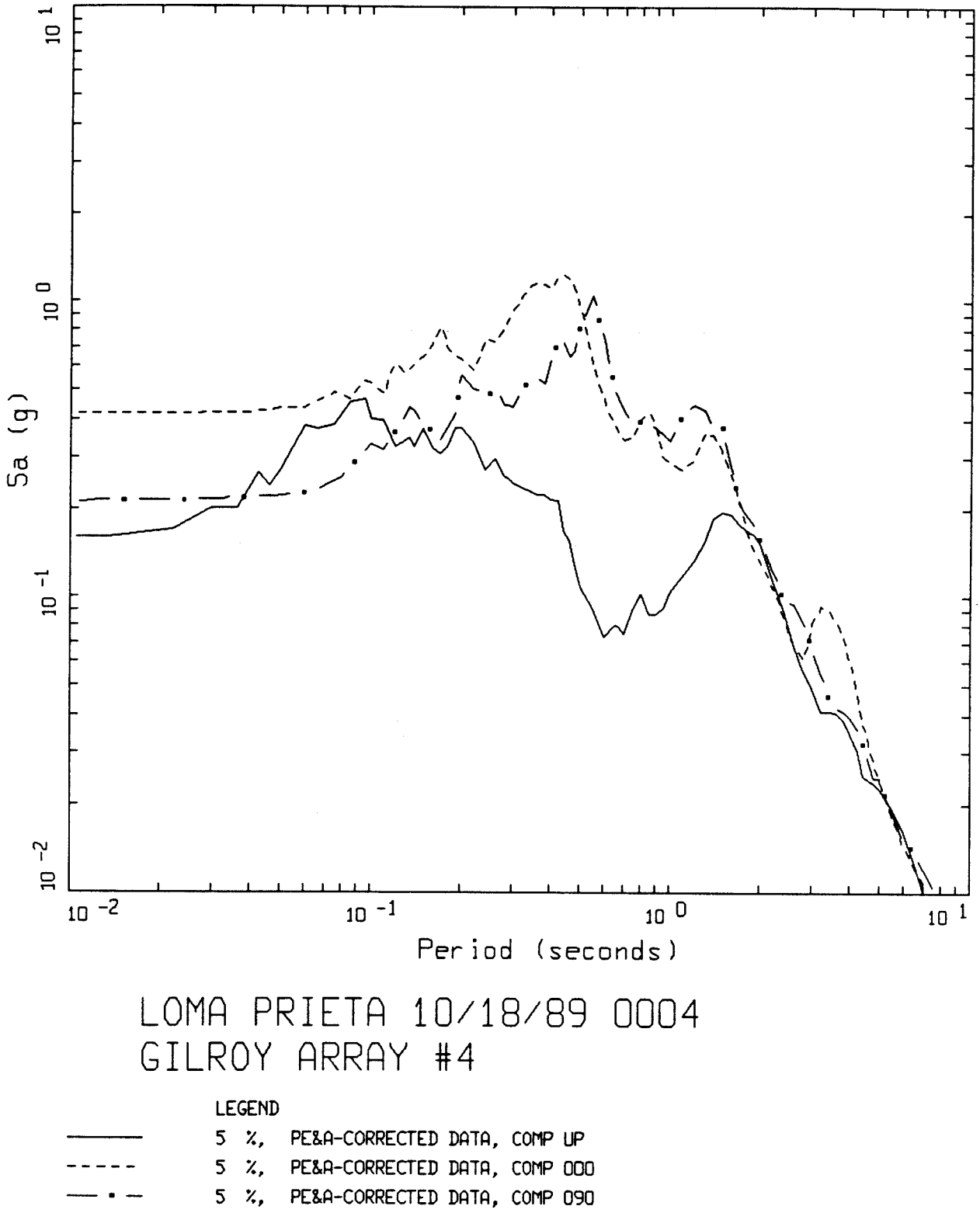

Figure 17. 5% Damped pseudo absolute response spectra at the soil site Gilroy 4 for the 1989 M 6.9 Loma Prieta earthquake. Fault distance is about 16 km.

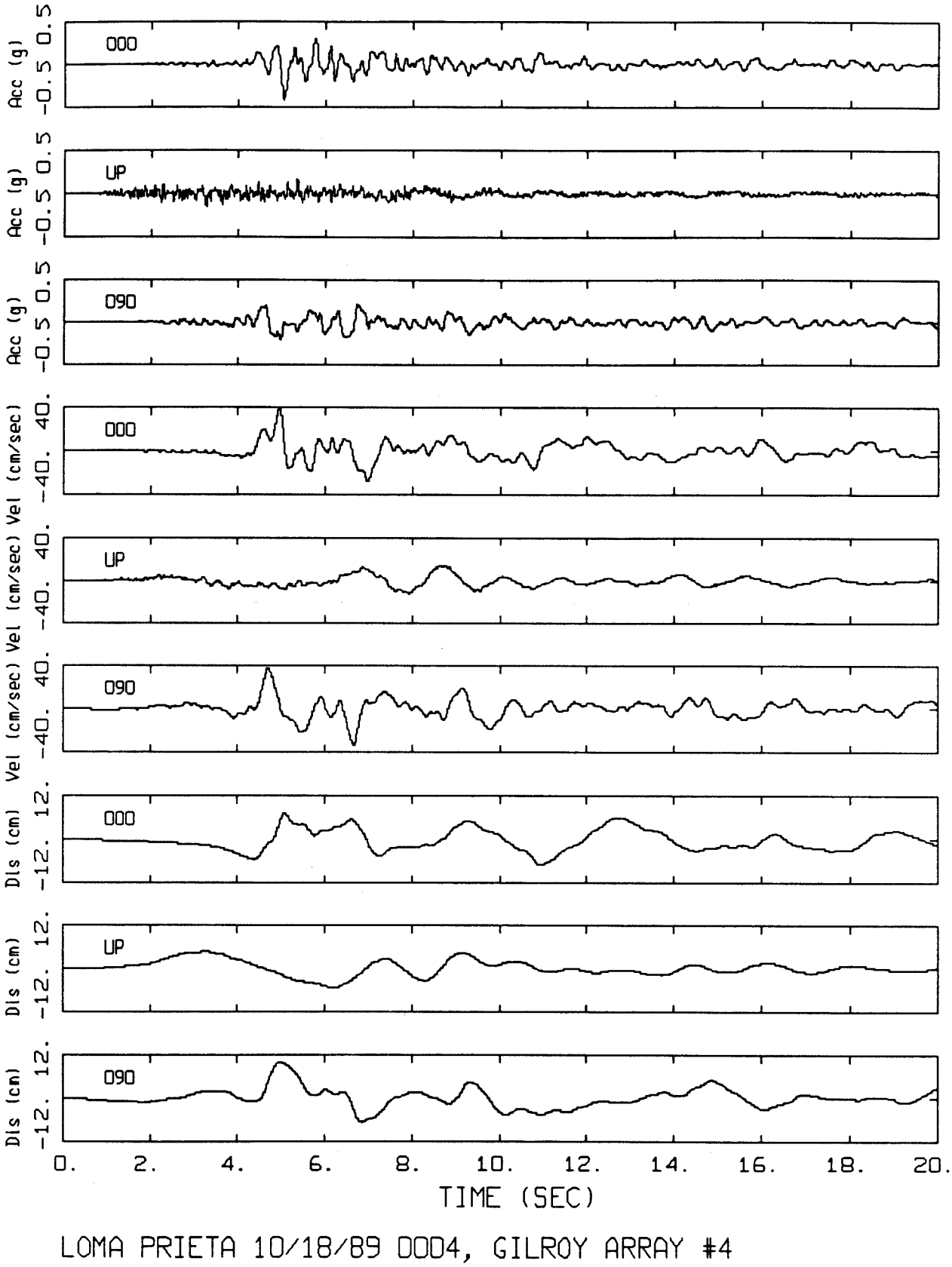

Figure 18. Acceleration, velocity, and displacement time histories at the soil site Gilroy 4 for the 1989 **M** 6.9 Loma Prieta earthquake. Fault distance is about 16 km.

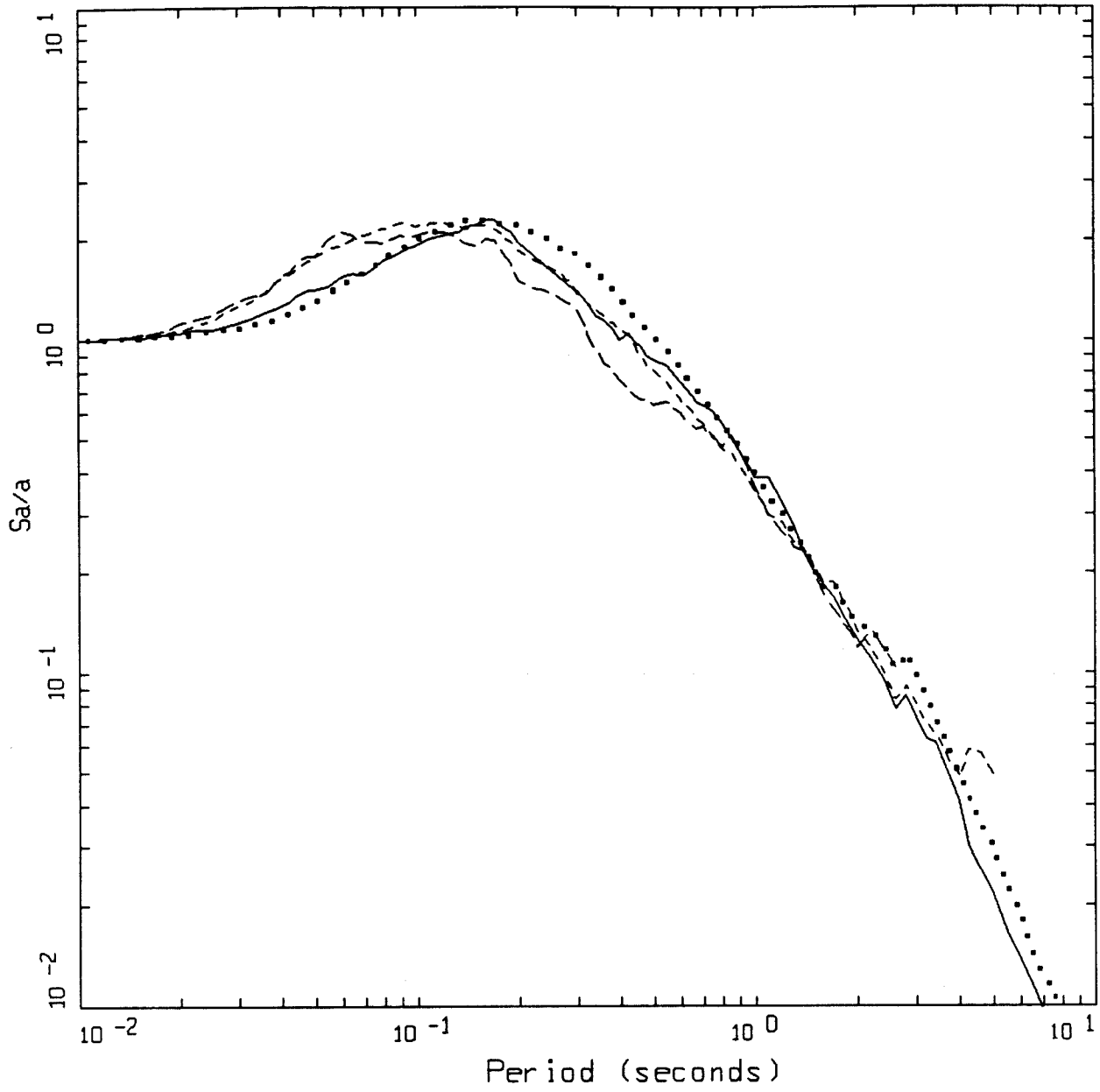

MEDIAN SPECTRAL SHAPES
M=5.5 (5.0-6.0), ROCK

LEGEND

HORIZONTAL, M=5.51 (5.0-6.0), D=7.84 KM (0-10 KM), AVG PGA = 0.179 G, 28 REC.

HORIZONTAL, M=5.59 (5.0-6.0), D=21.70 KM (10-50 KM), AVG PGA = 0.108 G, 182 REC.

VERTICAL, M=5.51 (5.0-6.0), D=7.84 KM (0-10 KM), AVG PGA = 0.124 G, 13 REC.

VERTICAL, M=5.59 (5.0-6.0), D=21.70 KM (10-50 KM), AVG PGA = 0.067 G, 88 REC.

Figure 19. Median statistical response spectral shapes (5% damping) computed from WUS data recorded at rock sites in the magnitude range of M 5 to M 6. Rupture distances range from 0 to 10 km and 10 to 50 km.

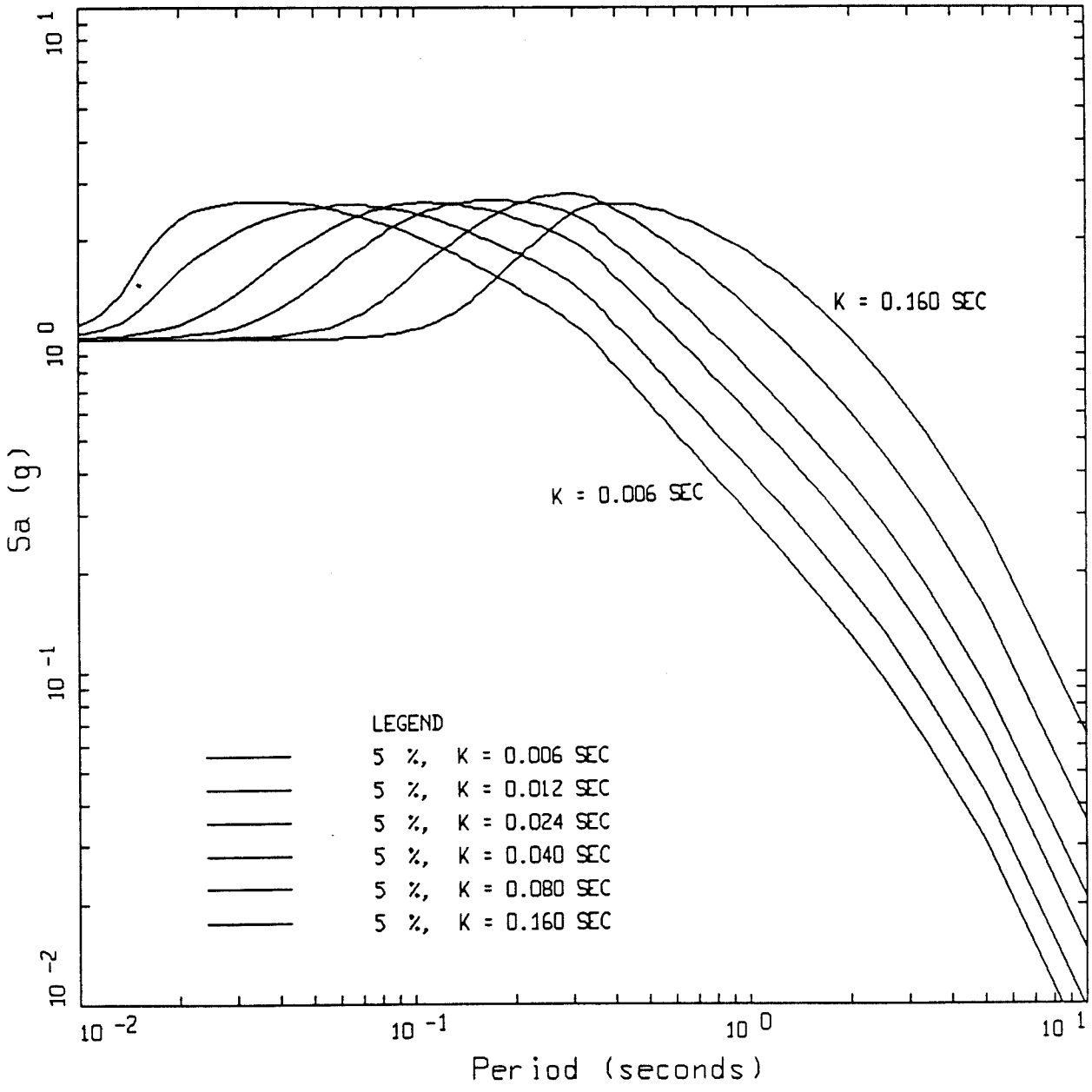

Figure 20. The effects of kappa on 5% damped response spectral shapes computed for a M 6.5 earthquake at 10 km using WNA parameters. As kappa increases, the peak shifts to longer periods and remains essentially constant in amplitude.

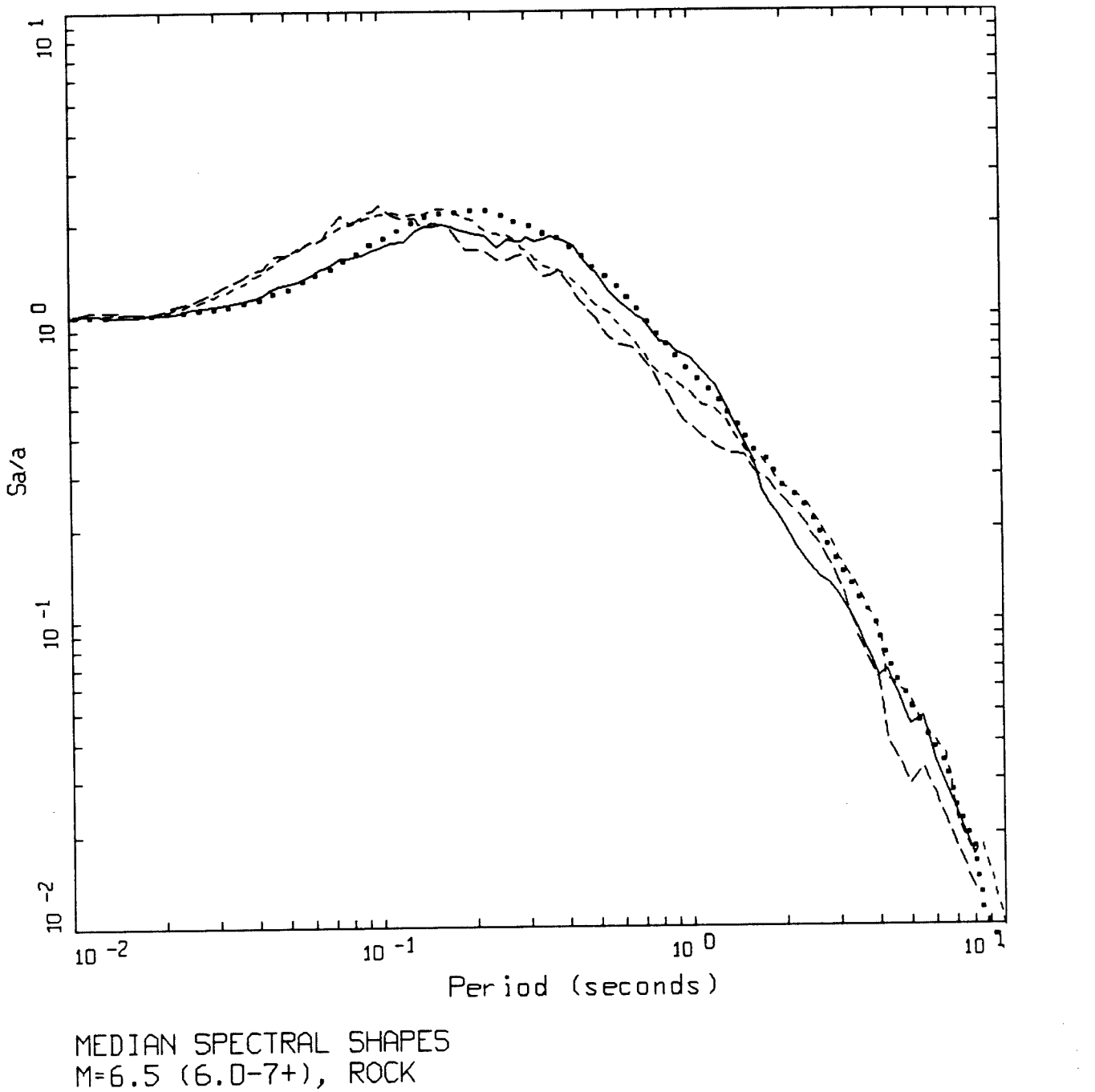

Figure 21. Median statistical response spectral shapes (5% damping) computed from WUS data recorded at rock sites in the magnitude range of M 6 to M 7+. Rupture distances range from 0 to 10 km and 10 to 50 km.

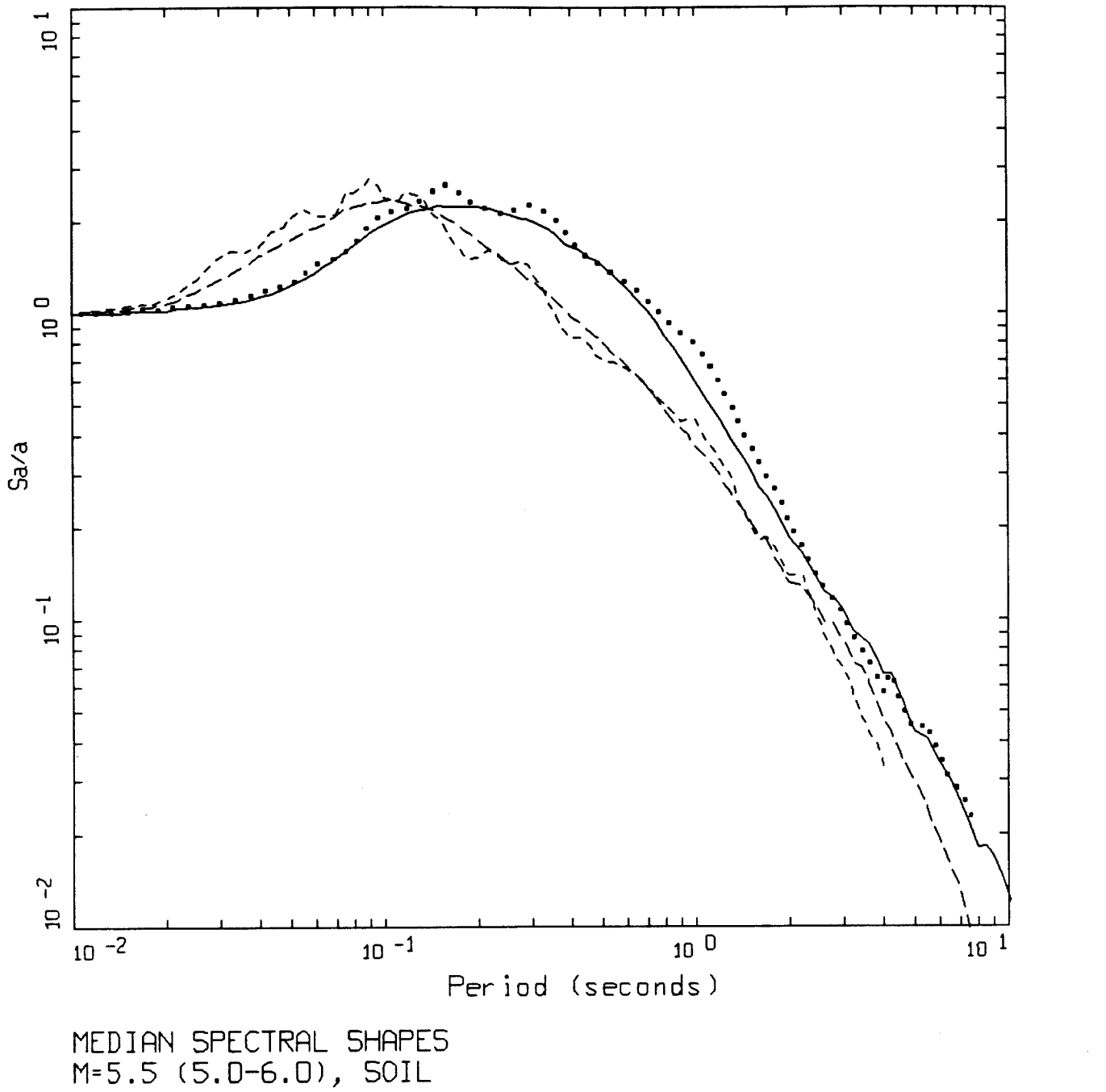

Figure 22. Median statistical response spectral shapes (5% damping) computed from WUS data recorded at soil sites in the magnitude range of M 5 to M 6. Rupture distances range from 0 to 10 km and 10 to 50 km.

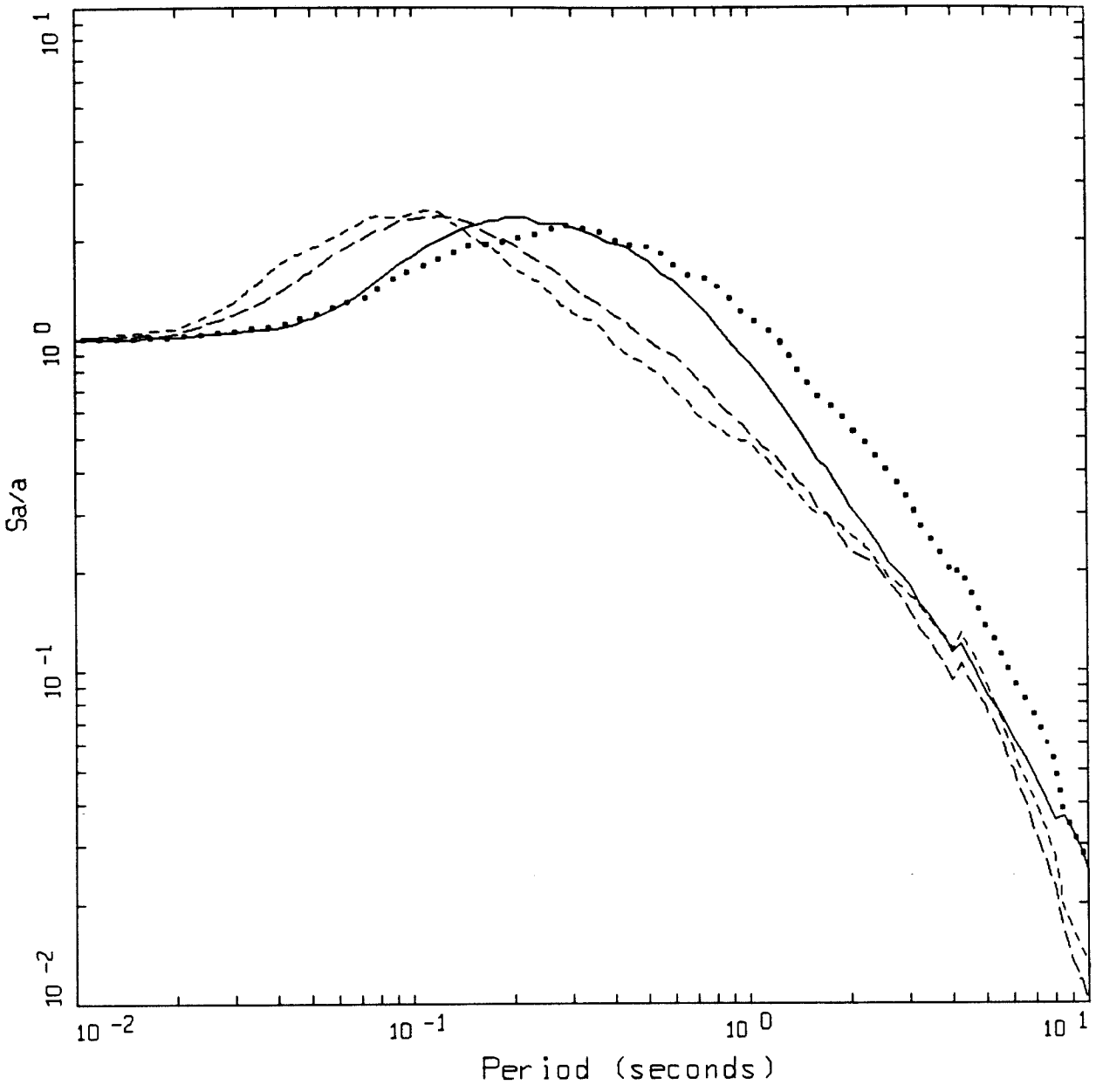

MEDIAN SPECTRAL SHAPES
M=6.5 (6.0-7.0), SOIL

LEGEND

• • • •	HORIZONTAL, M=6.51 (6.0-7.0), D=5.56 KM (0-10 KM), AVG PGA = 0.381 G, 87 REC.
———	HORIZONTAL, M=6.33 (6.0-7.0), D=28.49 KM (10-50 KM), AVG PGA = 0.136 G, 505 REC.
- - - - -	VERTICAL, M=6.51 (6.0-7.0), D=5.56 KM (0-10 KM), AVG PGA = 0.315 G, 42 REC.
— — — —	VERTICAL, M=6.33 (6.0-7.0), D=28.49 KM (10-50 KM), AVG PGA = 0.089 G, 247 REC.

Figure 23. Median statistical response spectral shapes (5% damping) computed from WUS data recorded at soil sites in the magnitude range of M 6 to M 7+. Rupture distances range from 0 to 10 km and 10 to 50 km.

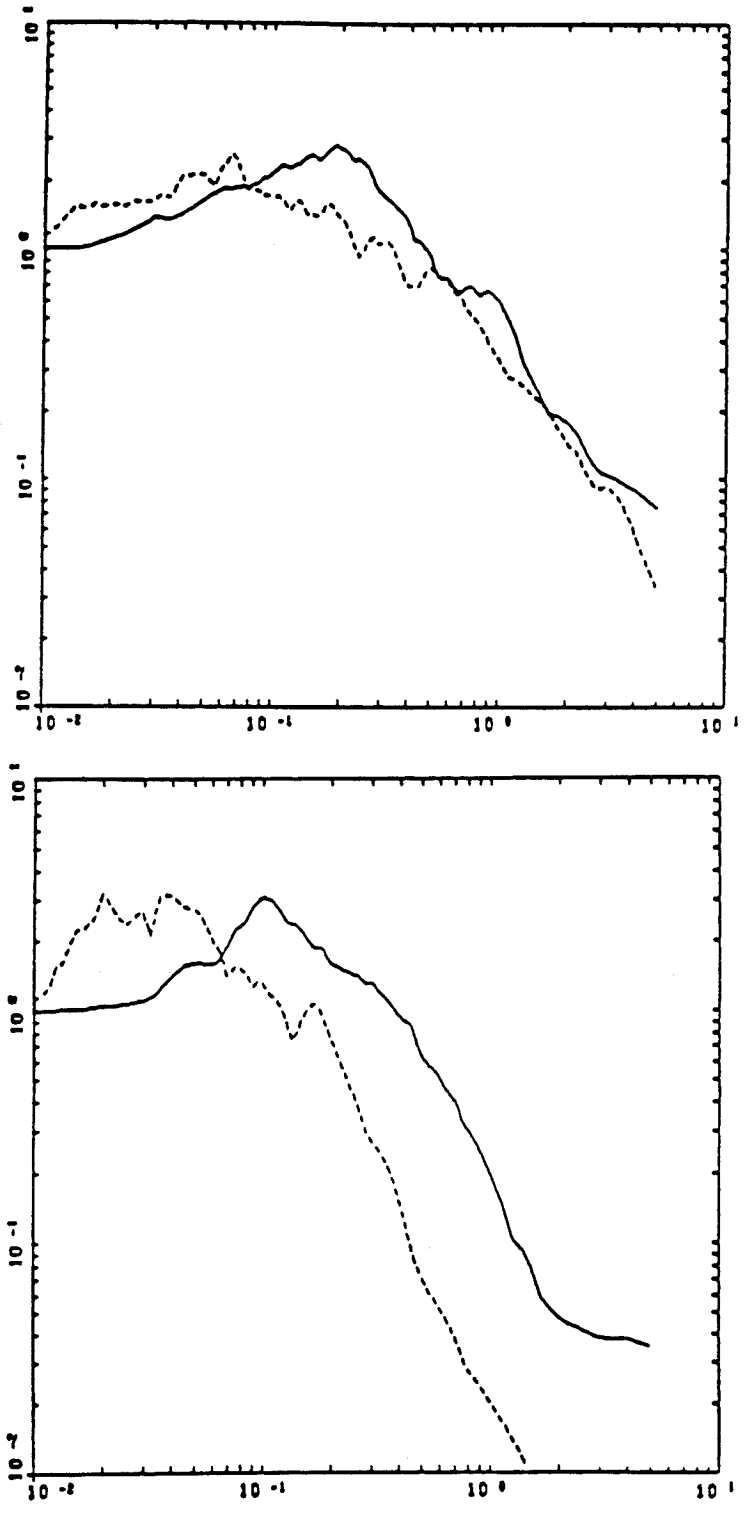

Figure 24. Average 5% damping response spectral shapes (Sa/a) computed from motions recorded on rock sites at close distances to M = 6.4 earthquakes (top figure) and M = 4.0 earthquakes (bottom figure). In each figure the solid line corresponds to motions recorded in WNA, dashed line to motions recorded in ENA.

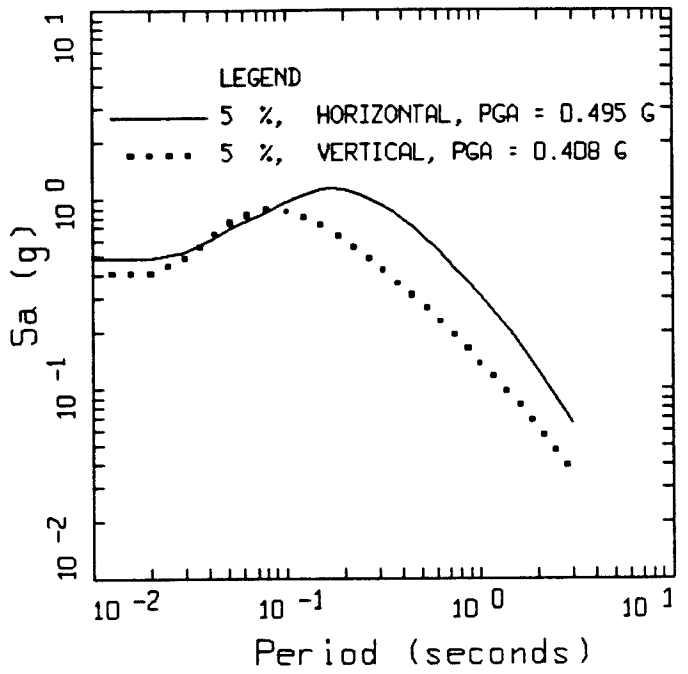

M = 6.5, ROCK
D = 5 KM

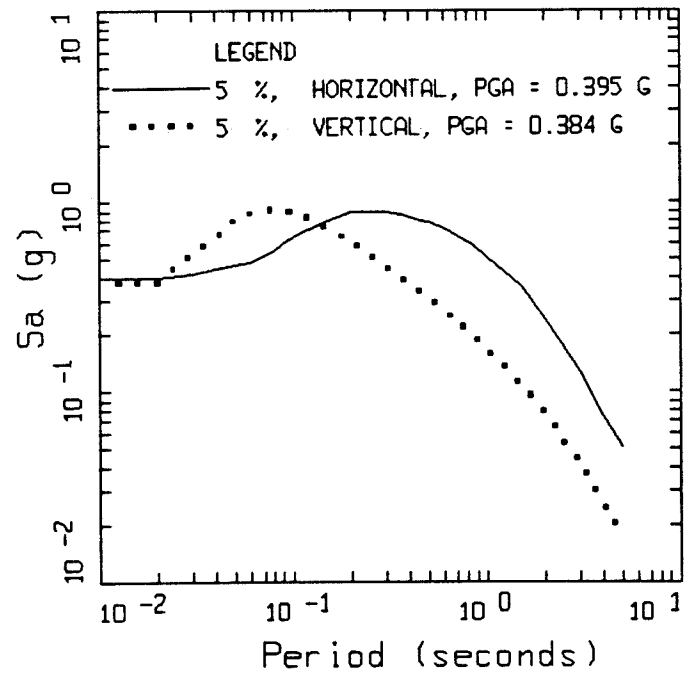

M = 6.5, SOIL
D = 5 KM

Figure 25. Median empirical response spectra (5% damped) computed at rock and soil sites for M 6.5 at a fault distance of 5 km.

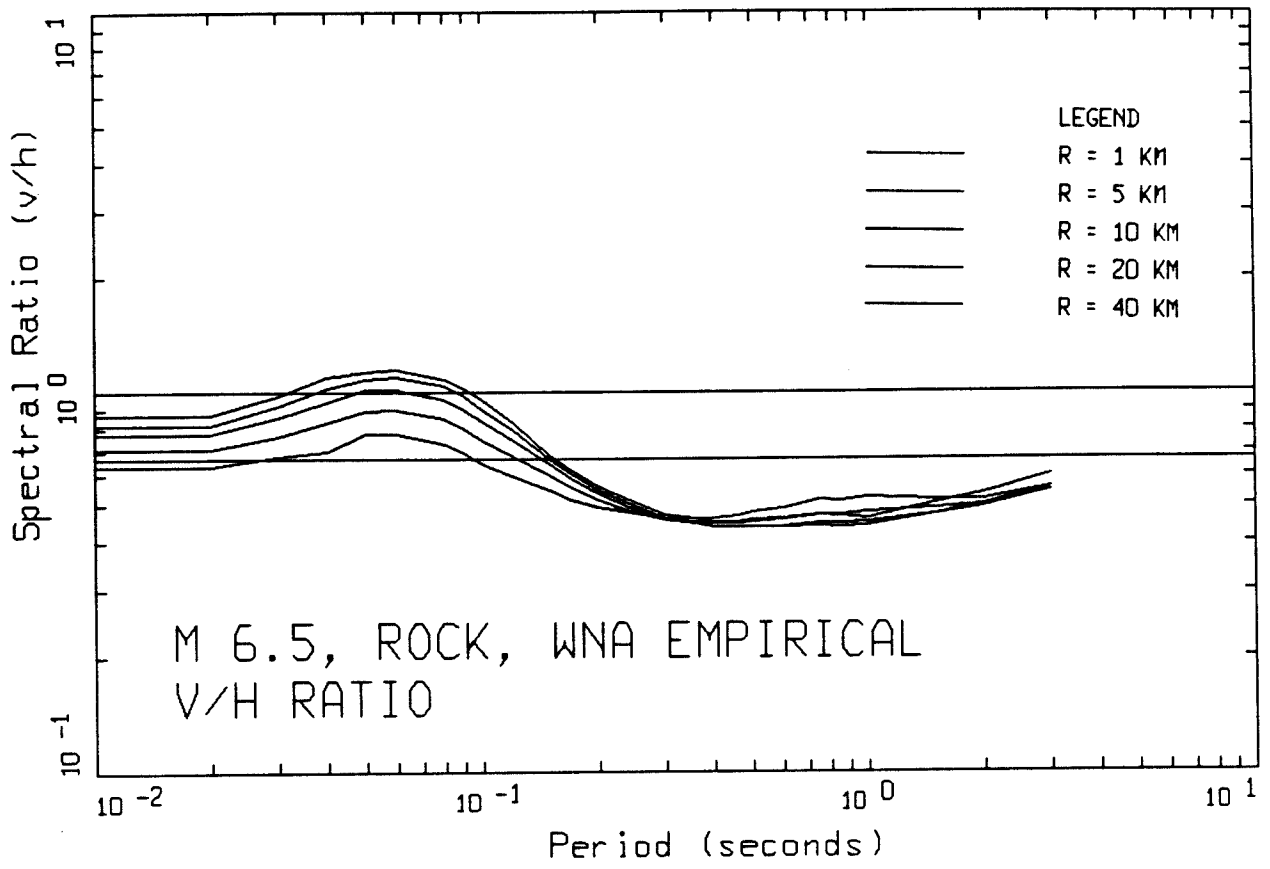

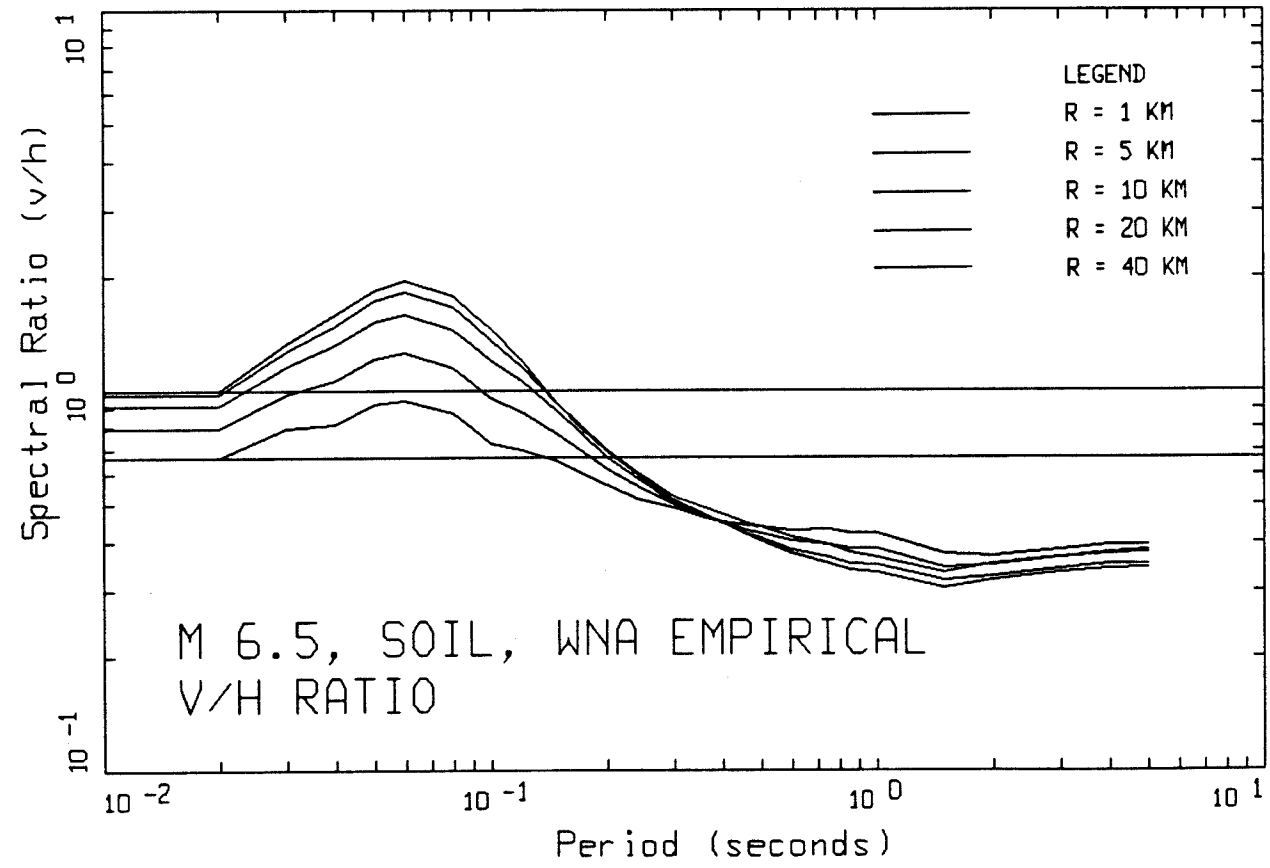

Figure 26. Distance (fault) dependency of response spectral ratios (V/H) for M 6.5 at rock and soil sites. Line at 0.66 indicates the constant ratio of 2/3.

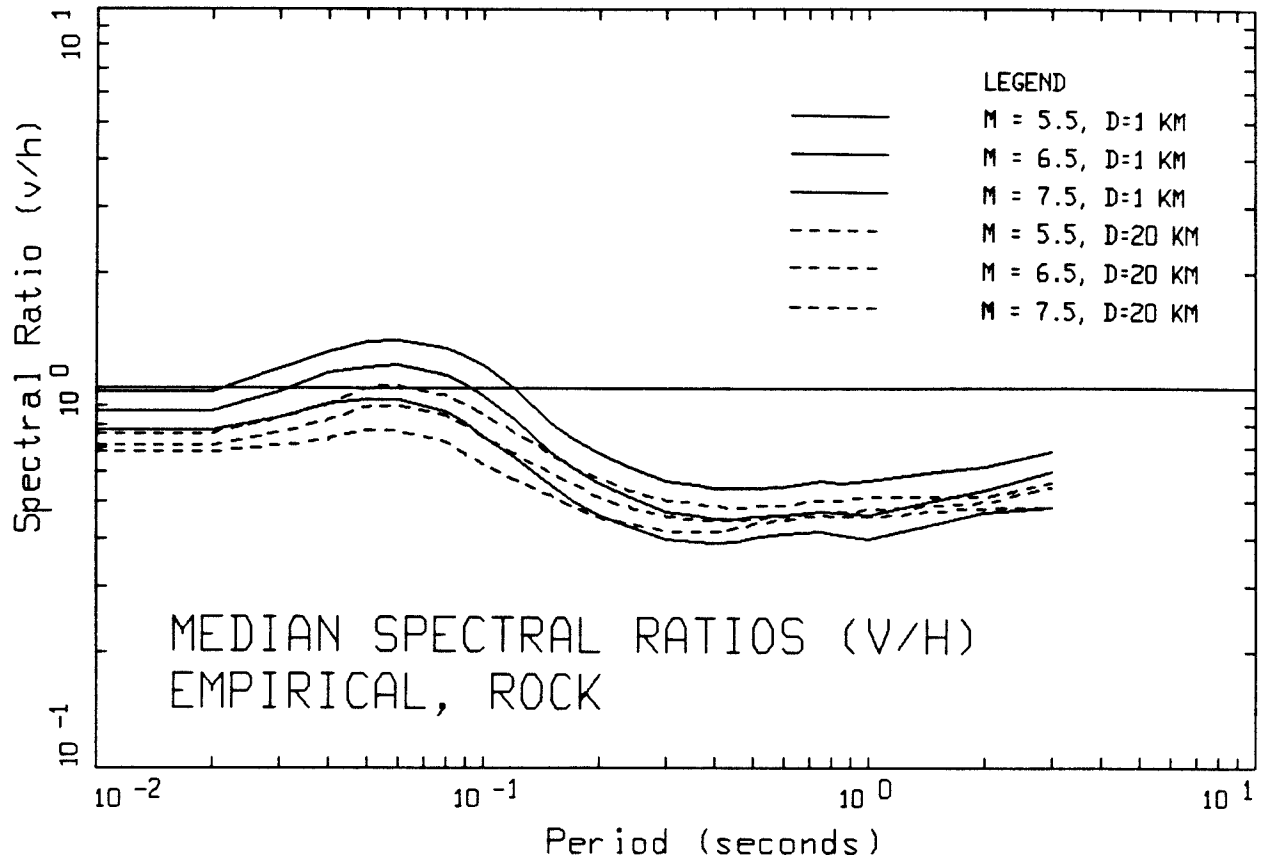

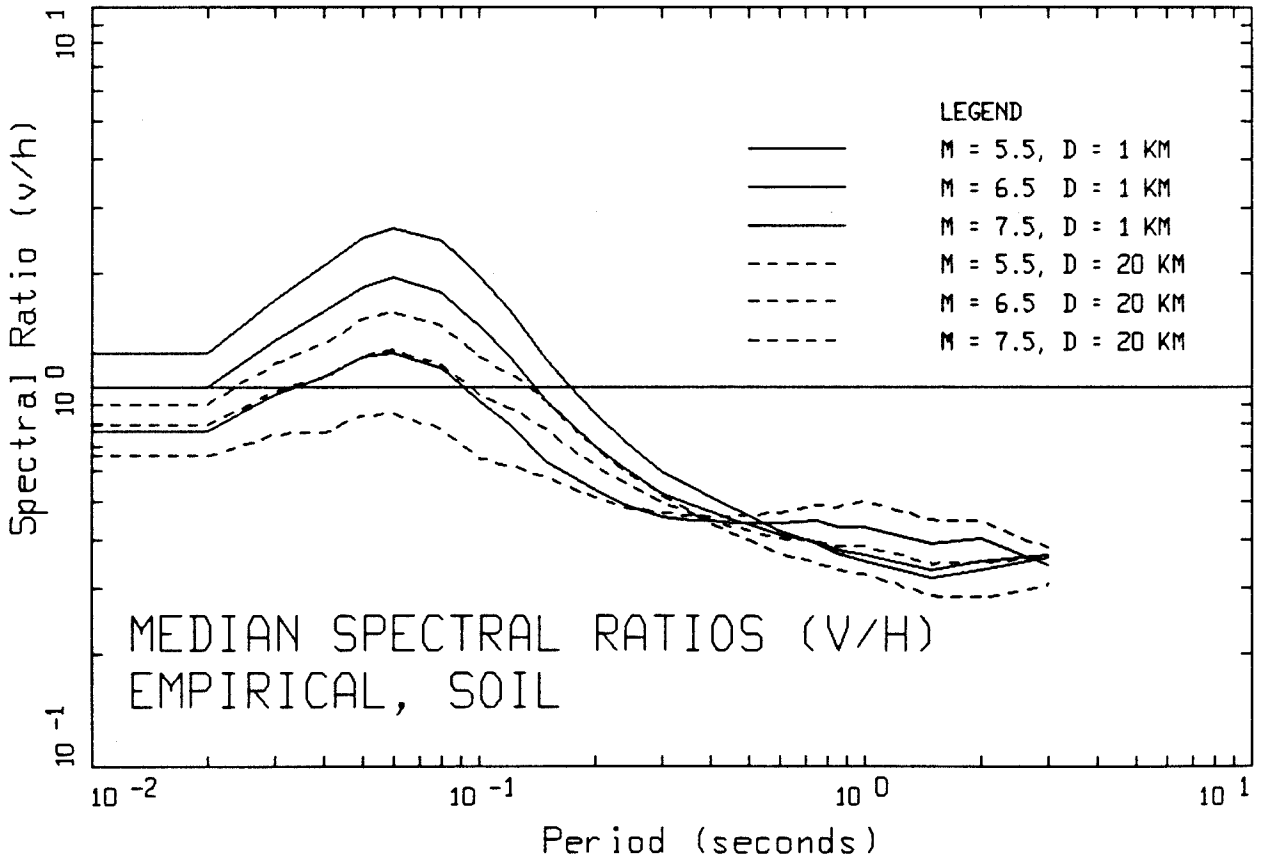

Figure 27. Magnitude dependency of response spectral ratios (V/H) at fault distances 1 and 20 km.

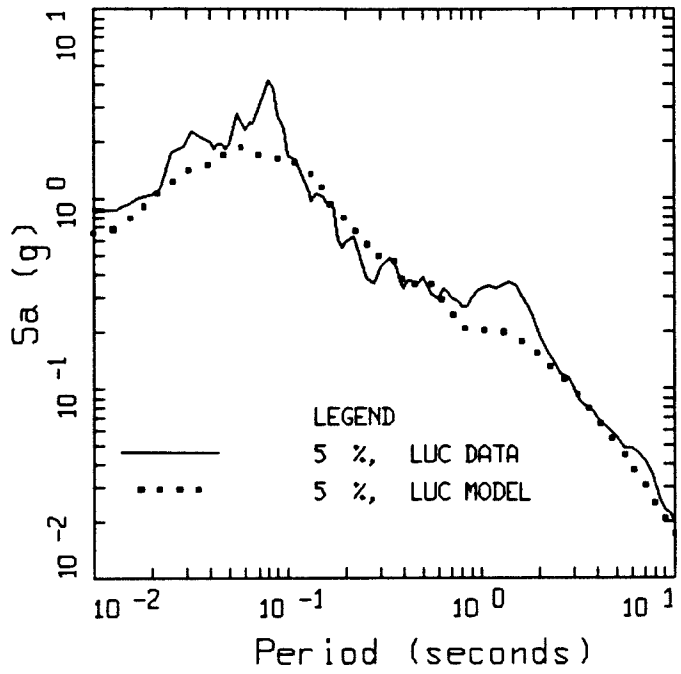

LANDERS, VERTICAL
LUC

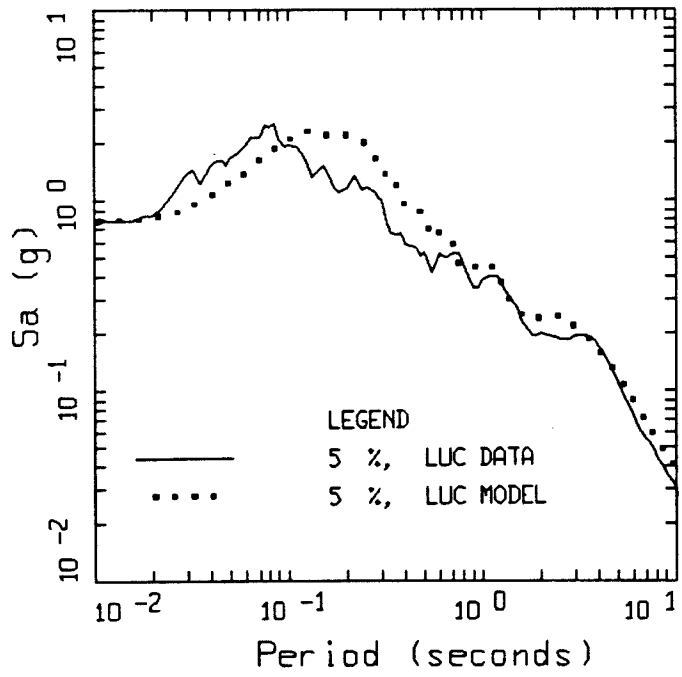

LANDERS, HORIZONTAL
LUC

Figure 28. Comparison of simulations to recorded motions for vertical and horizontal (average) components at the SCE rock site Lucerne for the 1992 M 7.2 Landers earthquake. The site is at a fault distance of about 2 km. A point-source model is used with the generic rock compression- and shear-wave velocity profiles (Figure 1) over the regional crustal model (Wald and Heaton, 1994).

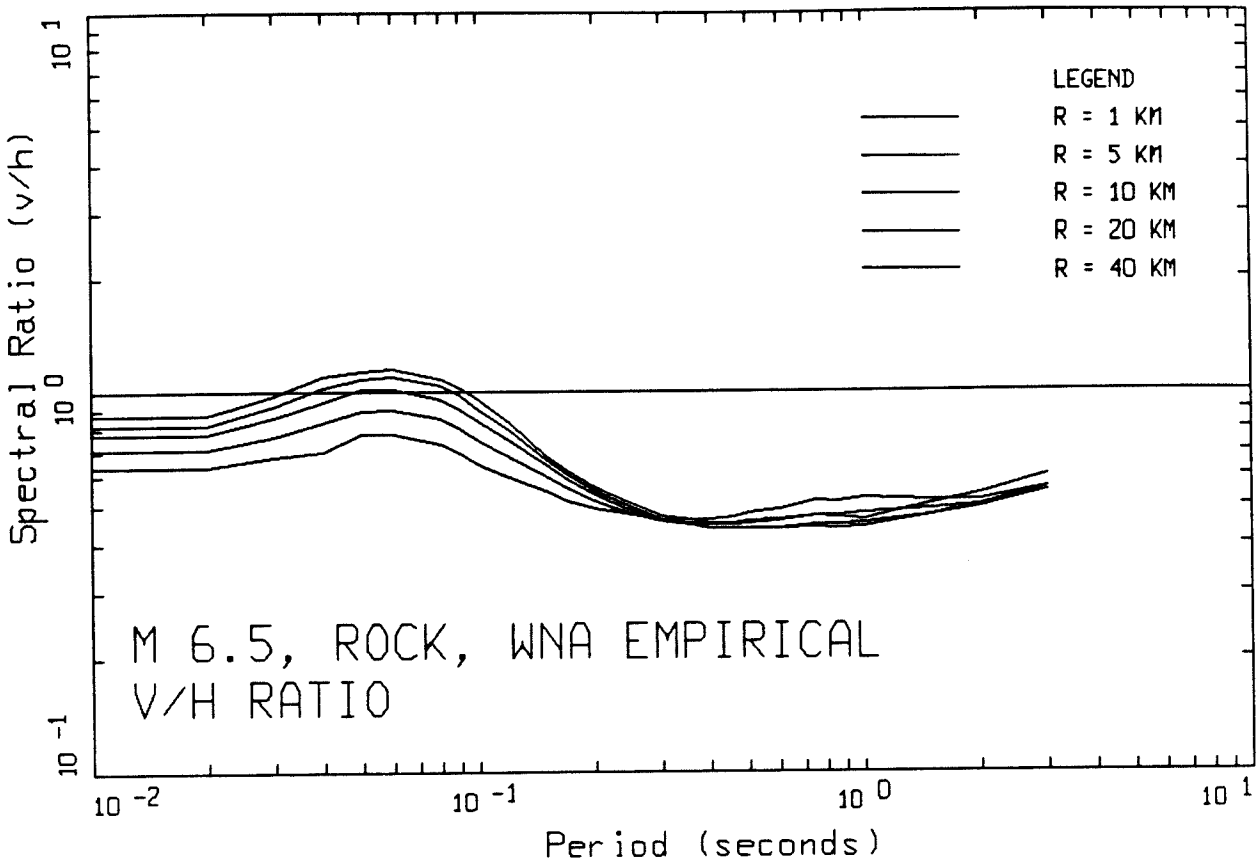

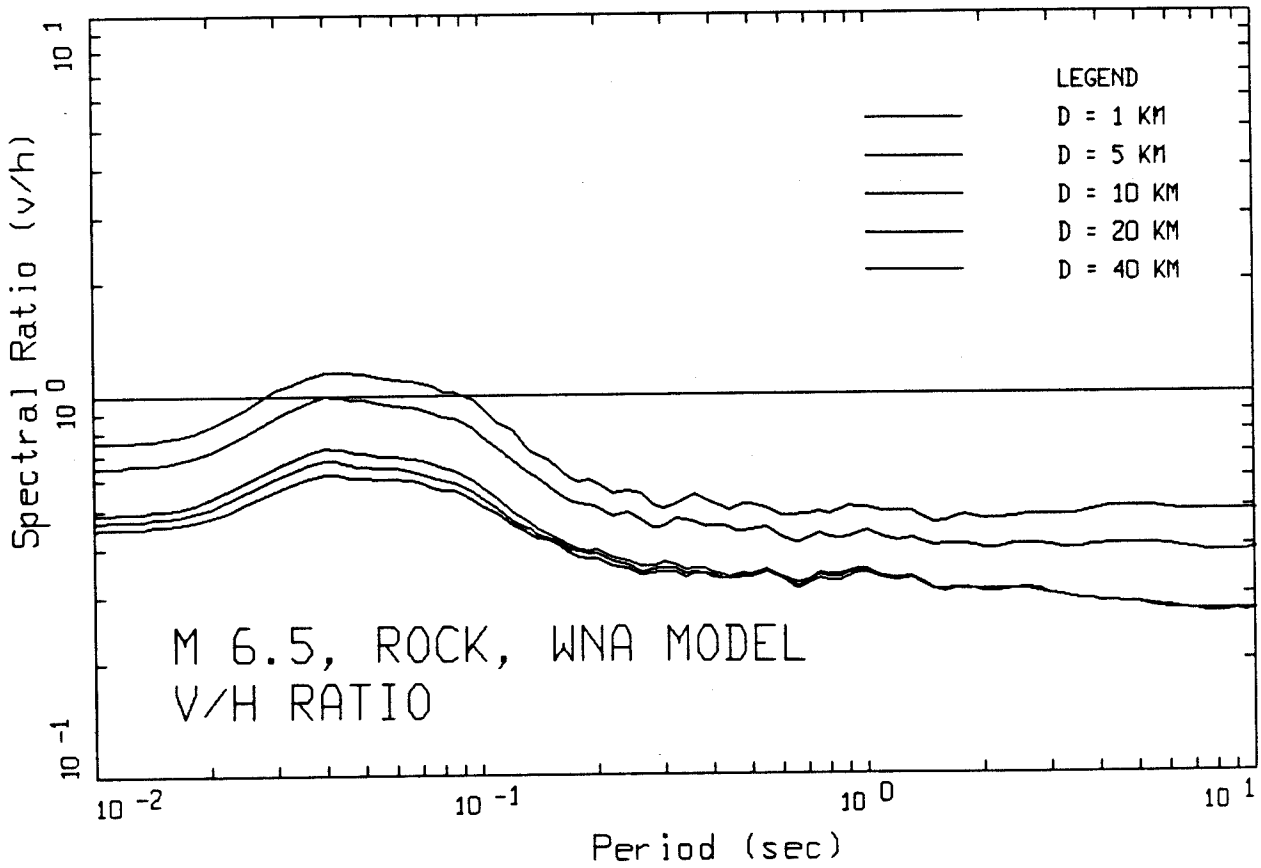

Figure 29. Comparison of empirical and model response spectral ratios (V/H) at rock sites for **M** 6.5.

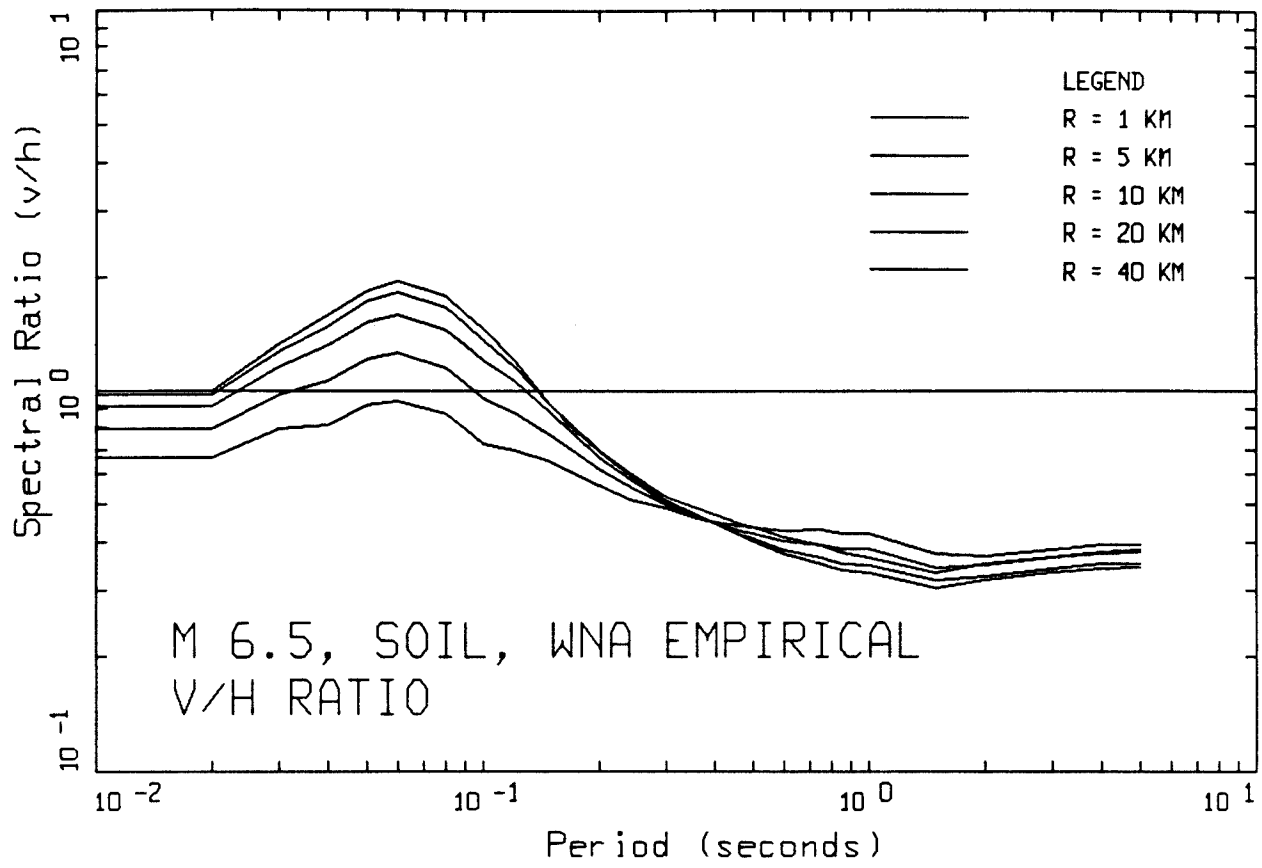

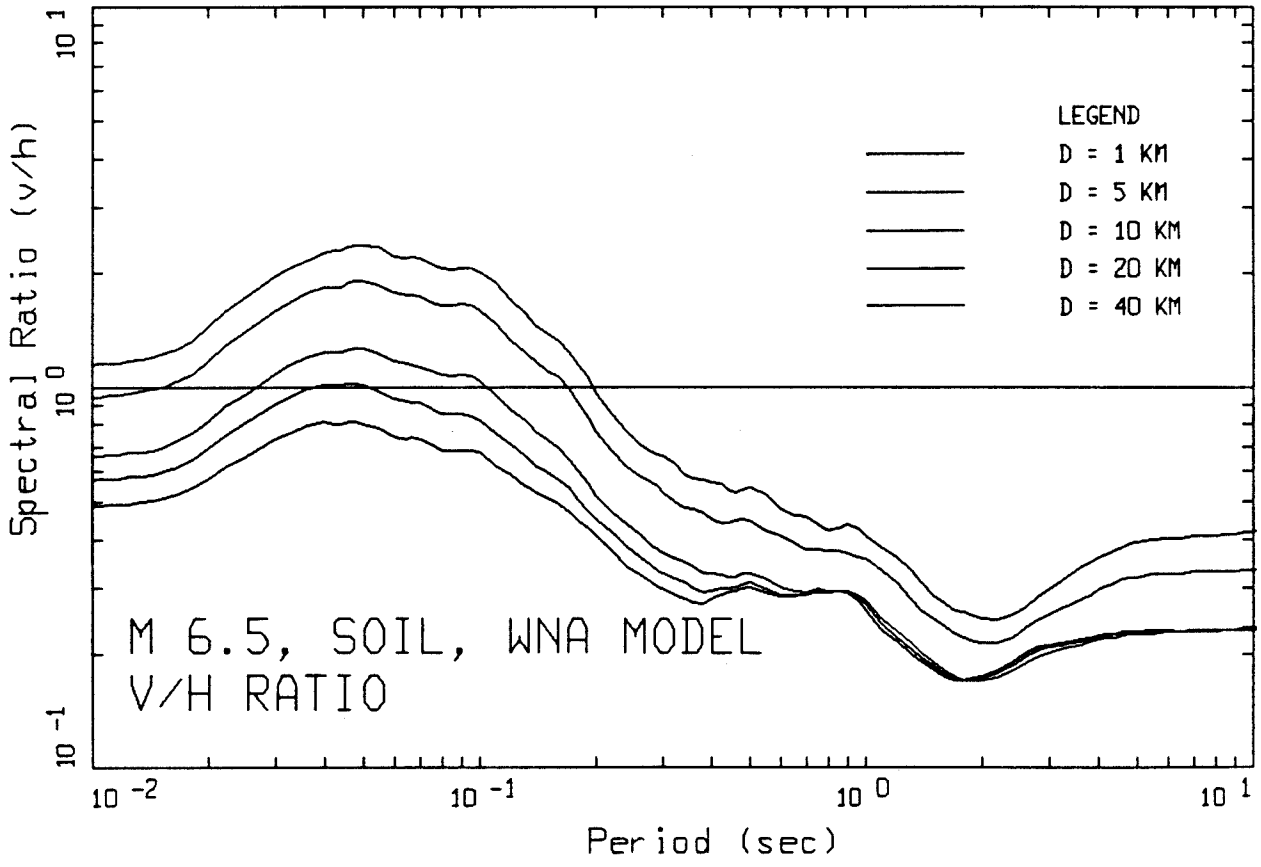

Figure 30. Comparison of empirical and model response spectral ratios (V/H) at soil sites for M 6.5.

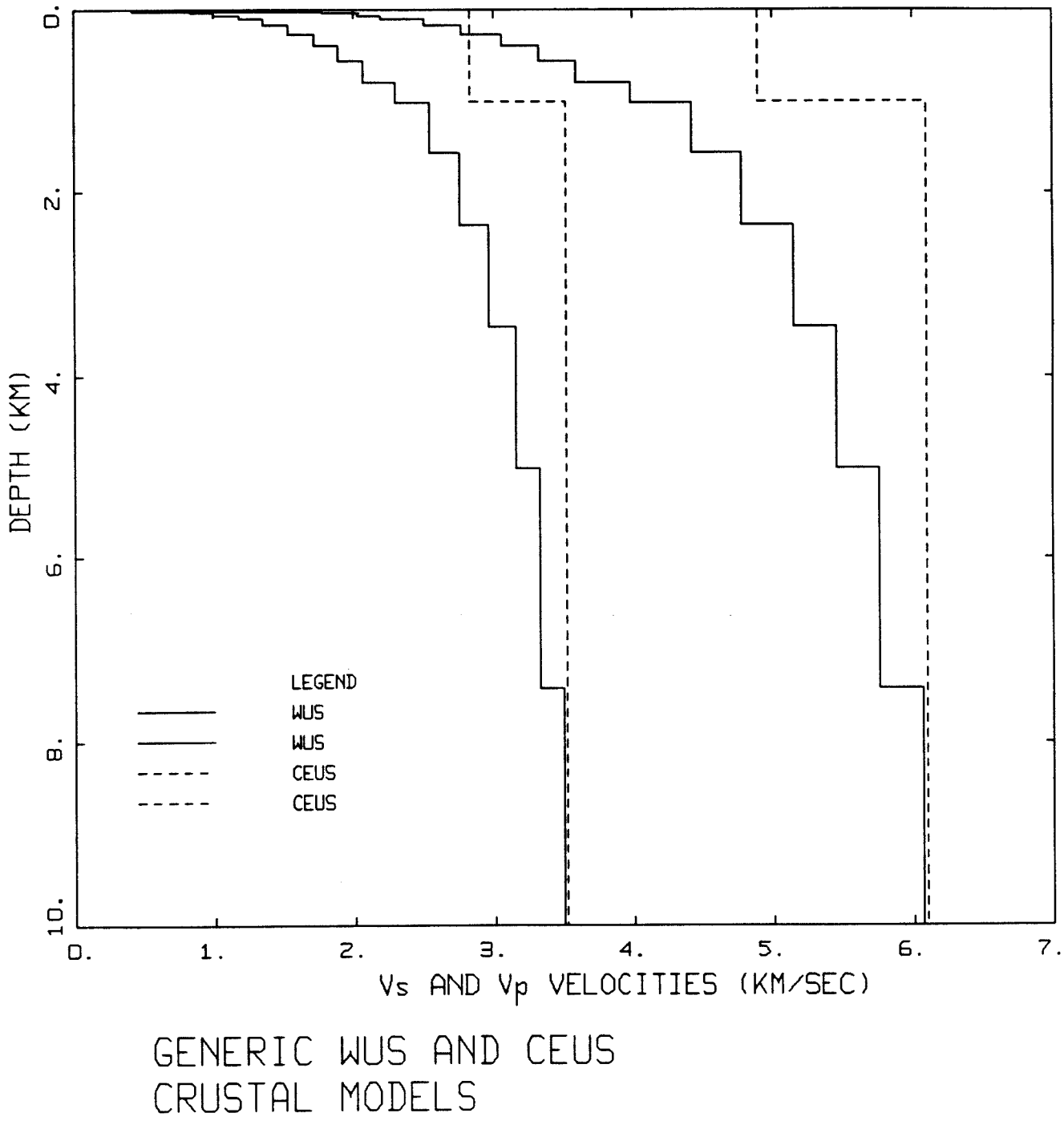

Figure 31. Comparison of generic compression- and shear-wave velocity profiles for WUS and CEUS crustal conditions.

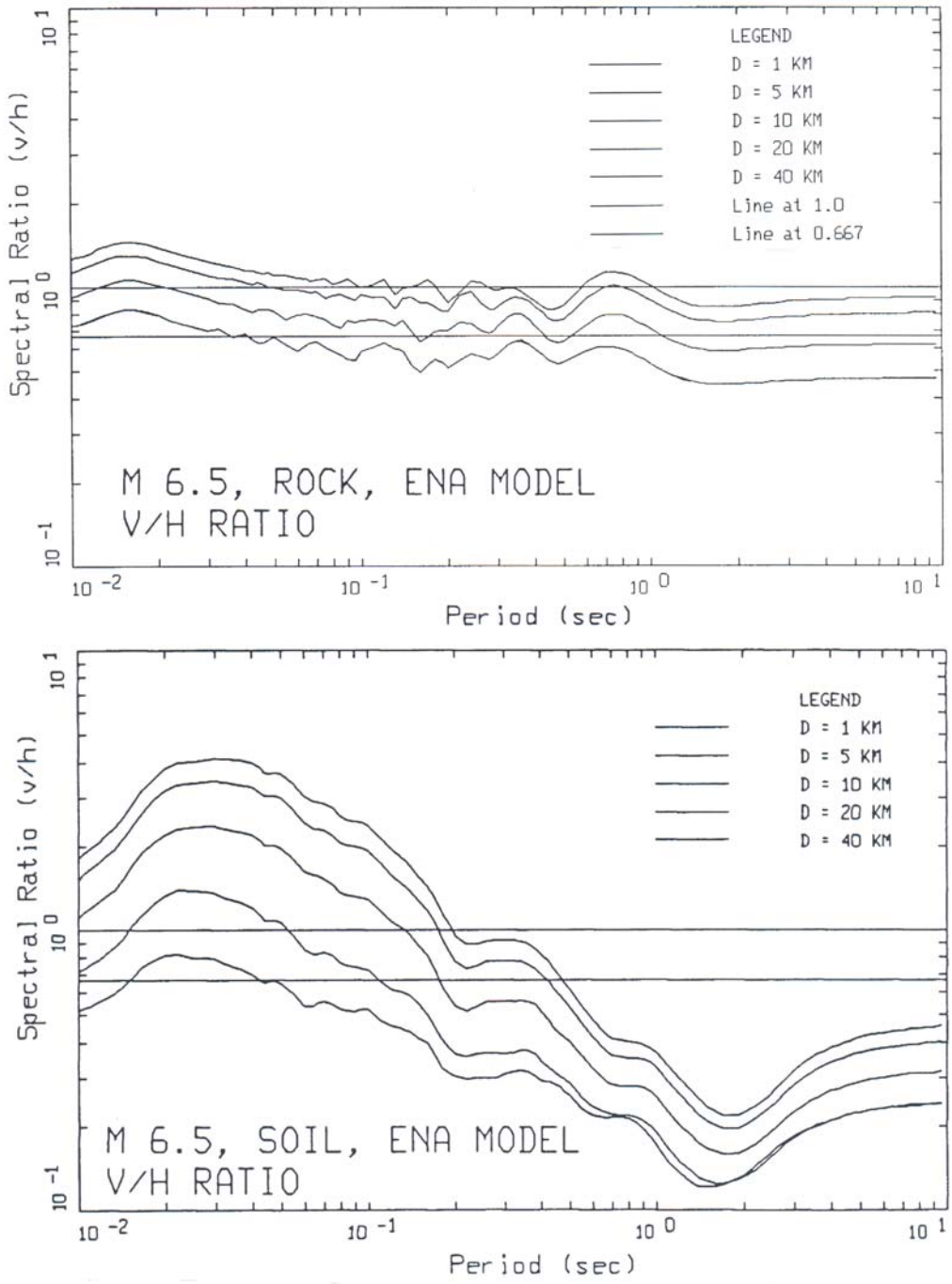

Figure 32. Response spectral ratios (V/H) computed for CEUS rock and soil sites for **M** 6.5 at a suite of distances. The CEUS crustal model (Figure 31) is used for rock sites with the generic soil profile (Figure 2) placed on top to model soil sites.